Journal of Neuroinflammation

RESEARCH

Open Access

Role of FPR2 antagonism in alleviating social isolation-induced depression and protecting blood-brain barrier integrity

Jiayi Zheng[1], Hanqi Wang[1], Wanning Wu[1], Linlin Wang[1], Meizhen Qin[2], Lingfeng Zhu[1,3], Zhen Liu[1], Yijun Chen[1] and Yang Yu[1*]

Abstract

Social isolation (SI) is a prevalent issue in modern society, particularly exacerbated during the COVID-19 pandemic, and it is a significant contributor to depressive disorders. Inflammation-related markers are upregulated in patients with major depressive disorder (MDD) unresponsive to first-line selective serotonin reuptake inhibitor (SSRI) antidepressants. This study investigates the role of formyl peptide receptor 2 (FPR2), a G-protein coupled receptor expressed in central and peripheral immune cells, in SI-induced depression. We developed a mouse model of SI by housing mice individually for three weeks. SI mice exhibited increased capillary-associated microglia (CAMs) with upregulated FPR2 expression in the prefrontal cortex (PFC) and hippocampus compared to group-housed controls. Notably, subcutaneous administration of the FPR2 antagonist WRW4 alleviated depressive and anxiety-like behaviors in SI mice, reducing microglial activation and neuronal damage. WRW4 treatment decreased CAM numbers and their FPR2 expression. RNA sequencing revealed that SI primarily induced changes in genes associated with blood-brain barrier (BBB) function, followed by alterations in genes related to hormone activity, immune activation, and neuronal function. Transcriptomic changes in brain endothelial cells from SI mice resembled those observed in animal models of several neurological disorders and in MDD patients. WRW4 treatment partially reversed these transcriptomic alterations and restored compromised BBB integrity. Additionally, intracerebroventricular (ICV) injection of WRW4 also alleviated depressive and anxiety-like behaviors in SI mice. Finally, our analysis of public transcriptome databases indicates FPR2 upregulation in the orbital ventral PFC of MDD patients and peripheral blood mononuclear cells of those in severe depressive episodes. These findings suggest that the pharmacological targeting of FPR2 may rescue SI-induced pathology in mice by protecting BBB integrity.

Keywords Social isolation, Major depressive disorder, Formyl peptide receptor 2, Microglia, Capillary-associated microglia, Brain-blood barrier, Brain endothelial cells, RNA sequencing, Plasma membrane monoamine transporter, Protocadherin

*Correspondence:
Yang Yu
yuyang2011@sjtu.edu.cn

Full list of author information is available at the end of the article

Graphical Abstract

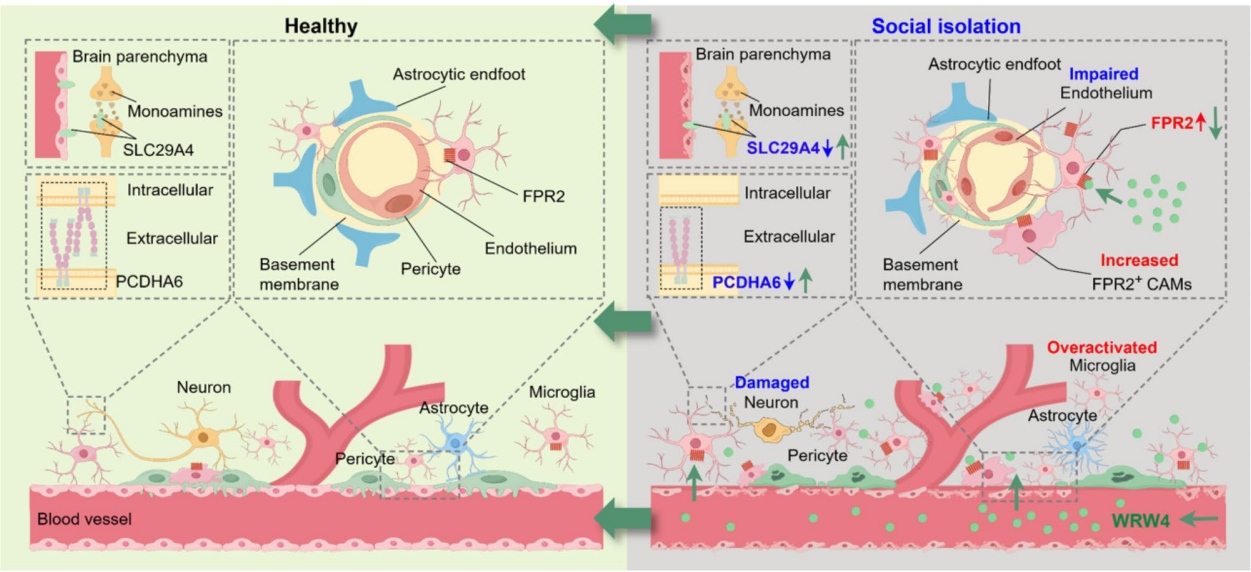

Background

Perceived Social isolation (i.e., loneliness) is prevalent in modern society [1]. It increases the risk of coronary heart and cerebrovascular diseases [2, 3], as well as mortality [4], and is also a significant contributor to mental disorders [5]. Individuals experiencing social isolation generally exhibit poorer mental health, and they are more likely to suffer from depression [6, 7]. Depression is the most common neuropsychiatric disorder, impacting over 300 million people globally [8]. Recent research has found that social isolation resulting from the COVID-19 pandemic has exacerbated the prevalence of depression and anxiety [9–11].

The pathogenesis of depression remains unclear. Currently used first-line drugs, such as selective serotonin reuptake inhibitors (SSRIs), exhibit heterogeneous therapeutic effects on patients with major depressive disorder (MDD) [12]. Studies have found elevated inflammatory markers in MDD patients who are unresponsive to these first-line antidepressants [13, 14]. Accumulating evidence supports the notion that the dysregulation of the immune system, including both central and peripheral immune responses, may play a critical role in the onset and progression of depression [15–17]. Alterations in the numbers of various immune cell types, a sustained low-grade pro-inflammatory state, and abnormal antibody titers have been observed in the peripheral blood of patients with depression [15, 16, 18]. In addition, the activation of immune cells, such as microglia, and increased expression of pro-inflammation factors have been documented in the brain tissue of MDD patients [19, 20]. The causal relationship between central and peripheral immunity in the pathogenesis of depression is still unclear. Given that depression is a multifactorial psychiatric disorder, it is speculated that their relationship may be bidirectional causality and mutually reinforcing, thereby facilitating the pathological progression of depression.

Additionally, impairment of the blood-brain barrier (BBB) and increased permeability have been observed in the brains of patients with depression [21–23]. The BBB, a component of the cerebral vasculature, is a highly selective and semipermeable membrane of endothelial cells that regulates the transfer of solutes and chemicals between the blood circulation and the central nervous system (CNS) [24]. It is a crucial barrier that protects and maintains brain homeostasis and serves as an essential channel for communication between the peripheral and central immune systems [25]. The BBB is formed by endothelial cells lining the capillary wall, pericytes embedded within the capillary basement membrane, and astrocyte endfeet wrapping the capillaries [26]. The neurovascular unit (NVU) also includes microglial cells and neurons [26, 27]. Microglia, the brain's resident immune cells, play a dual role in modulating BBB permeability following systemic inflammation [28]. Recent studies have revealed that under physiological conditions, approximately one-third of microglial cells make physical contact with vasculature through more stable microglial cell bodies. These microglia are referred to as capillary-associated microglia (CAMs) [29]. Research has shown that in depressed patients, brain endothelial cells are compromised, as evidenced by a reduction in tight junction proteins and functional changes in pericytes and astrocytes

[21–23]. However, the changes in CAMs and their role in BBB in depression require further clarification.

Human formyl peptide receptor 2 (FPR2) is a G protein-coupled receptor that belongs to the FPR family, which also includes the subtypes FPR1 and FPR3 [30]. FPR2 is expressed in various cell types, including peripheral immune cells as well as central microglia and neurons [31, 32]. It plays a critical role in innate immunity, host defense, and inflammatory responses, contributing significantly to both peripheral and central immune processes [33–36]. FPR2 recognizes various endogenous or non-endogenous (including synthetic) ligands with varying sizes and structures. These ligands range from proteins (such as annexin A1 [ANXA1]) and peptides (N-formyl peptides, Ac2-26 [N-terminal peptide of ANXA1], WKYMVm [W peptide], WRWWWW [WRW4], and Boc-2) to lipids (lipoxin A4 [LXA4] and resolvin D1 [RvD1]) and small molecules (Quin-C1) [37]. Upon ligand binding, FPR2 activates downstream ligand-specific signaling pathways and cellular responses, resulting in either pro-inflammatory or anti-inflammatory (pro-resolving) effects [38–42]. The role of FPR2 in psychiatric disorders is largely unknown. Research has demonstrated that the intracerebroventricular (ICV) injection of FPR2 agonist RvD1 alleviates depressive-like behaviors in LPS-induced depressed mice and chronic unpredictable stress model mice [43, 44]. Other studies have found that *Fpr2/3* knockout mice exhibit increased exploratory and decreased fearful behaviors compared to wild-type (WT) mice, and the FPR2 antagonist Boc-2 partially mimics these behaviors [45]. Furthermore, FPR2/3 deficiency mitigates depressive-like behaviors and cognitive deficits in mice induced by corticosterone administration [46]. These findings suggest that FPR2 is involved in the pathological progression of depression and may represent a potential target for depression treatment. However, the regulatory mechanisms of FPR2 and the roles of its various ligands in depression warrant further investigation.

In this study, we first established a mouse model of depression induced by social isolation and assessed the changes in FPR2 expression in the brains of mice, particularly in CAMs. Various ligands of FPR2 were administered individually to the socially isolated (SI) mice. Notably, the peptide antagonist WRW4, rather than the agonists Ac2-26 or W peptide, alleviated the depressive and anxiety-like behaviors in SI mice. Additionally, WRW4 treatment reduced neuroinflammatory responses and improved neuronal functions in these mice. Subsequently, RNA sequencing was conducted on the prefrontal cortex (PFC) of the mice to elucidate the molecular and cellular mechanisms by which WRW4 improves depressive-like behaviors and related biochemical indicators in SI mice. Finally, alterations in FPR2 expression in the central and peripheral blood of MDD patients were validated using public transcriptomic databases.

Methods

Antibodies and reagents

Primary antibodies used in this study are listed in Table 1. FPR2 antagonist WRW4 and agonists Ac2-26 and W peptide (> 95% purity) were synthesized at Genscript Biotech Corporation (Piscataway, NJ, USA). The BCA protein assay kit and 4, 6-diamidino-2-phenylindole (DAPI) were obtained from Beyotime Biotech Inc (Nantong, China). Nissl staining solution was from Yeasen Biotechnology (Shanghai, China). AlexaFluro-488-conjugated anti-rabbit IgG and AlexaFluor-555-conjugated anti-rat IgG secondary antibodies (Cat.No. A21206 and A21434, respectively) were purchased from Invitrogen (Waltham, MA, USA). AlexaFluor-647-conjugated anti-rabbit IgG secondary antibody (Cat.No. ab150079) was from Abcam (Cambridge, UK). HRP-labeled Goat Anti-Mouse IgG and HRP-labeled Goat Anti-Rabbit IgG were from ALLWIN Biotechnology Co., Ltd. (Shanghai, China). Other chemicals were purchased from Sigma-Aldrich, Inc. (St. Louis, MO, USA).

Table 1 Primary antibodies used in this study

Antibody	Type	Specificity	Reference/Source	Catalog Number
FPRL1/AF647	Poly	FPRL1	Bioss	bs-3654R-AF647
Iba1	Poly-	Iba1	FUJIFILM Wako Pure Chemical	019-19741
Iba1	Mono-	Iba1	Abcam	ab178846
CD31	Poly-	CD31	BD Biosciences	550,274
GFAP	Mono-	GFAP	Proteintech	16825-1-AP
GFAP-Cy3™	Mono-	GFAP	Sigma-Aldrich	C9205
SYN	Poly-	Synaptophysin	Proteintech	17785-1-AP
PSD95	Poly-	PSD95	Bioss	bs-0179R
SLC29A4	Poly-	SLC29A4	Bioss	bs-4176R
PCDHA6	Poly-	PCDHA6	Proteintech	12853-1-AP
Albumin	Poly-	Albumin	Bioss	bs-2256R
GAPDH	Mono-	GAPDH	Proteintech	60004-1-1 g

Animals

The male C57BL/6J mice were purchased from Shanghai Slaccas Laboratory Animal Co., Ltd. (Shanghai, China). All mice were group-housed (4–5 mice per cage) with a 12-h light-dark cycle and ad libitum access to food and water. Housing, breeding, and experimentation procedures were conducted following the guidelines outlined in the National Institutes of Health Guide for the Care and Use of Laboratory Animals and were approved by the Biological Research Ethics Committee of Shanghai Jiao Tong University (Protocol number: 202101323/Approval date: 14 October 2021).

Social isolation procedure

Mice aged 6 weeks at the beginning of the experiment were randomly divided into five groups: group-housed (GH), socially isolated (SI), SI with WRW4 treatment (SI + WRW4), SI with Ac2-26 treatment (SI + Ac2-26), and SI with W peptide treatment (SI + W peptide) groups. The GH group consisted of 4–5 mice per cage with unrestricted access to food and water. The other four groups of mice underwent 3 weeks of social isolation, during which each mouse was housed individually in a cage, allowing it to hear and smell neighboring mice while preventing any visual contact or physical interaction with other mice [47].

Drug administration

For peripheral administration, WRW4 (1.5 mg/kg), Ac2-26 (0.5 mg/kg), or W peptide (1.5 mg/kg) was subcutaneously injected on days 15, 17, 19, and 21 after social isolation modeling. The selection of dosages for these agents was based on previously published studies [48–50]. All reagents were dissolved in a solution of 30% DMSO and 70% sterile saline before administration. Mice in the GH and SI groups received equivalent volumes of the solution via subcutaneous injection. The body weight of the mice was measured every 2–3 days. On the 22nd day of post-modeling, behavioral tests were conducted on the mice from all five groups.

For central administration, WRW4 was administered via intracerebroventricular (ICV) injection on day 18, and behavioral tests were conducted on day 21 after social isolation modeling. Mice were deeply anesthetized using sodium pentobarbital (45 mg/kg, i.p.) and subsequently restrained onto a stereotaxic apparatus. Each mouse in the SI + WRW4 group received a single ICV injection of 5 μg WRW4, delivered in a total volume of 8 μl. The WRW4 solution was freshly prepared in 0.9% saline and administered bilaterally into the lateral ventricles of the brain. The coordinates for the bregma were established as follows: ±1.0 mm lateral, − 0.3 mm posterior, and − 1.5 mm below [51]. Mice in the GH and SI groups received an equal volume of 0.9% saline using the same method. After the surgery, all mice were maintained on heating pads (37 °C) until they recovered. Three days following the surgery, all mice were subjected to behavioral tests.

After the behavioral tests, all mice were anesthetized with sodium pentobarbital (45 mg/kg, i.p.), euthanized by decapitation, and their brains were removed immediately. The prefrontal cortices from the left hemisphere of the brain were isolated, flash-frozen in liquid nitrogen, and stored at − 80℃ for subsequent biochemical analyses and RNA sequencing. The right hemispheres of the brain were fixed with 4% paraformaldehyde (PFA) in 0.1 M phosphate-buffered saline (PBS), then underwent cryoprotection in 30% sucrose. Sagittal sections of 30 μm thickness were prepared using a freezing sliding microtome. Sections were preserved in a glycol anti-freeze solution (consisting of 12.5 g/L polyvinylpyrrolidone (average MW 40,000), 375 g/L saccharose, 375 mL/L glycol, and 625 mL/L Tris-buffered saline (TBS, 0.1 M, with 12.1 g/L Tris-base, 40 g/L NaCl)) at − 20 °C. For the immunofluorescence staining and biochemical analyses, each group included 3–5 mice.

Behavioral tests

Tail suspension test (TST)

In the tail suspension test, each mouse was suspended approximately 35 cm above the ground by tape about 1 cm from the tail tip. The mice were separated from each other with baffles during suspension to prevent mutual interference. A total test duration of 6 min was conducted, with immobility duration in the final 4 min recorded as a measure of despair behavior. Immobility was defined as the absence of tail and limb movement. The immobility time was recorded using an automated video tracking system (TopScan, CleverSys Inc., Reston, VA, USA).

Forced swim test (FST)

The forced swim test was performed in a transparent glass cylinder with a diameter of 18 cm and a height of 27 cm. The water depth was 15 cm, and the temperature was kept at 23–25 °C. Each mouse was gently placed in the water tank. Baffles were placed between adjacent cylinders to prevent the mice from seeing each other. The water in the cylinder was refreshed every three mice to avoid interference from excreta. Immobility duration within the 6 min was monitored using an automated video tracking system (TopScan) and analyzed for the final 4 min. Mice were considered immobile when they ceased swimming and remained passively afloat with their heads above the water's surface. After swimming, the mice were removed from the water, gently dried, and returned to their home cages.

Sucrose preference test (SPT)

The sucrose preference test consists of three stages: (1) Adaptation stage: 2% sucrose solution was prepared and placed in the cages of mice for 12 h. (2) Fasting stage: mice were deprived of water and food for 12 h before testing. (3) Sucrose preference test: 2% sucrose and drinking water bottles were weighed and placed simultaneously on the cage. Mice can freely drink either liquid from the two bottles for 12 h. After the test, two bottles were weighed again, and the sucrose preference rate within 12 h was calculated. Sucrose preference rate (%) = sucrose consumption/total consumption × 100%.

Elevated plus maze test (EPM)

The elevated plus maze apparatus comprised four arms (30 × 5 cm) connected by a central 5 × 5 cm area. Two opposite-facing arms were open (open arms), while the other two were enclosed by 20 cm-high walls (closed arms). The entire maze was elevated to 80 cm above ground level. Mice were gently placed in the central area facing an open arm and allowed to explore the maze for 5 min. Entries into the open arms were tracked and analyzed using an automated video tracking system (TopScan). The maze floor was cleaned with 75% alcohol after each trial.

Open field test (OFT)

Exploratory activities and spontaneous locomotion were assessed by allowing mice to freely explore a polyvinyl chloride square arena (50 × 50 cm, 40 cm high walls) for 5 min. Each mouse was placed individually in the center of the arena, with a video camera mounted above and connected to a computer. The movement of mice was recorded using an automated video tracking system (TopScan), and the total distance traveled in the arena was analyzed.

Western blot

The mouse brain tissues were homogenized in RIPA lysis buffer (Beyotime) supplemented with protease and phosphatase inhibitors (Beyotime). Protein concentrations were determined using BCA Kits following the manufacturer's instructions. The homogenates were mixed with 5 × sodium dodecyl sulfate (SDS)-PAGE loading buffer, heated at 99 °C for 10 min, and separated into 10% or 15% SDS-PAGE gels. After separation, samples were transferred onto nitrocellulose membranes (GE Healthcare, Wauwatosa, WI, USA) and blocked with 5% non-fat milk for 1 h at room temperature. Then, the membranes were probed with primary antibodies, including anti-Iba1 (1:1000), anti-GFAP (1:5000), anti-PSD95 (1:1000), anti-SYN (1:10,000), anti-PCDHA6 (1:1000), anti-SLC29A4 (1:2000), and anti-GAPDH (1:20,000) overnight at 4 °C, followed by incubation with HRP-labeled Goat Anti-Rabbit IgG (H + L) or HRP-labeled Goat Anti-Mouse IgG (H + L) secondary antibodies. Membranes were imaged using an Amersham ImageQuant 800 imager (Cytiva, Marlborough, MA, USA). Densitometric quantification of protein bands was performed using ImageJ software (National Institutes of Health, Bethesda, MD, USA).

Immunofluorescence staining

Brain sections were performed for standard immunofluorescence staining. Briefly, the sections were rinsed with 0.05 M TBS, permeabilized with 0.1% Triton X-100 in TBS for 10 min, and blocked with 5% normal donkey serum in TBS (0.1% Tween-20) for 1 h at room temperature. For the detection of FPR2 expression in capillary-associated microglia (CAMs), the brain sections were first incubated with anti-CD31 (brain endothelial cell marker) antibody (1:200) overnight at 4 °C. Then, the sections were washed in TBS and stained with AlexaFluor-555-conjugated anti-rat antibody (1:500) for 1 h. After 3 TBS washes, the sections were incubated with anti-Iba1 antibody (1:200) overnight, rinsed in TBS, and stained with AlexaFluor-488-conjugated anti-rabbit antibody (1:500) for 1 h. The sections were washed in TBS and incubated with anti-FPRL1/AF647 antibody (1:200) for 1 h at room temperature, followed by counterstaining with DAPI for 10 min before mounting on glass slides.

To detect GFAP expression, brain sections were incubated with anti-GFAP-Cy3™ antibody (1:400) for 1 h at room temperature. The sections were subsequently rinsed in TBS and counterstained with DAPI for 10 min before mounting on glass slides.

For synaptophysin expression assessment, brain sections were first incubated overnight at 4 °C with anti-synaptophysin antibody (1:200). After rinsing in TBS, the sections were stained with Alexa Fluor 647-conjugated anti-rabbit antibody (1:500) for 1 h at room temperature. Then, the sections were washed in TBS, counterstained with DAPI for 10 min, and mounted on glass slides.

To assess the expression of albumin, PCDHA6, or SLC29A4 in brain endothelial cells, the brain sections were first incubated with anti-CD31 antibody (1:200) overnight at 4 °C, rinsed in TBS and then subjected to Alexa Fluor 555-conjugated anti-rat secondary antibody (1:500) for 1 h at room temperature. After three TBS washes, the sections were stained with anti-albumin antibody (1:200), anti-PCDHA6 antibody (1:200), or anti-SLC29A4 antibody (1:200) overnight at 4 °C, rinsed in TBS, and then incubated with Alexa Fluor 647-conjugated anti-rabbit secondary antibody (1:500) for 1 h. The sections were washed in TBS, counterstained with DAPI for 10 min, and mounted on glass slides.

The fluorescent confocal images were acquired using a laser-scanning confocal microscope (TCS SP8, Leica

Microsystems, Wetzlar, Germany, or LMS900, Carl Zeiss, Oberkochen, Germany). To quantify the expression of FPR2, CD31, Iba1, GFAP, Synaptophysin, SLC29A4, PCDHA6, and albumin, the relative immunofluorescence intensities were measured with the ImageJ software (National Institutes of Health). To assess microglial activation, microglial cell bodies were delineated, and their area was quantified using the ImageJ software (National Institutes of Health).

Colocalization analysis was performed using Manders' colocalization coefficients [52, 53] calculated via the Coloc2 plugin of Fiji software (National Institute of Health). Specifically, the M1 and M2 coefficients were determined using the following formulas:

$$M1 = \frac{\sum S1_{i,\ coloc}}{\sum S1_i} \in [0,\ 1]$$

$$M2 = \frac{\sum S2_{i,\ coloc}}{\sum S2_i} \in [0,\ 1]$$

Where $S1_{i,\ coloc}$ represents the fluorescence intensity of pixels in channel 1 that overlap with channel 2, and $S1_i$ is the total fluorescence intensity of channel (1) Similarly, $S2_{i,\ coloc}$ denotes the fluorescence intensity of pixels in channel 2 that overlap with channel 1, while $S2_i$ is the total fluorescence intensity of channel (2) The M2 coefficient was calculated as the ratio of the fluorescence intensity of Iba1 (channel 1) that overlapped with FPR2 (channel 2) to the total fluorescence intensity of FPR2 (channel 2). High M2 values indicate significant colocalization of Iba1 with FPR2. Conversely, the M1 coefficient was calculated as the ratio of the fluorescence intensity of PCDHA6, SLC29A4, or albumin (channel 2) overlapping with CD31 (channel 1) to the total fluorescence intensity of CD31 (channel 1). High M1 values signify significant colocalization of SLC29A4, PCDHA6, or albumin with CD31.

The 3D reconstructions of FPR2, microglia (Iba1), and blood vessels (CD31) were conducted using the Surfaces module in Imaris software (version 10.1, Bitplane, Zurich, Switzerland). Additionally, the Spots module was employed to quantify the number of microglia and CAMs. The fluorescence area of FPR2 within the CAMs and the average fluorescence intensity of Iba1 were quantified using the Surfaces module. The data are expressed as mean ± SEM, based on two distinct fields for each region, with three mice per group.

Nissl staining

Brain sections were stained with Nissl staining solution following the manufacturer's instructions. The sections were washed in double-distilled water and stained with Nissl staining solution at 37 °C for 1 h. The sections were then rinsed with double-distilled water for 5 s, decolorized in 95% alcohol for 5 s, dehydrated in a series of gradient ethanol solutions, and cover-slipped with neutral balsam. Images were captured using the bright field of a microscope (Olympus BX53, Tokyo, Japan) and quantified using ImageJ software (National Institutes of Health).

RNA sequencing (RNA-seq)

RNA extraction, library construction, sequencing, clean reads filtering, and gene abundance quantification were conducted by Shanghai Biotree Biomedical Technology Co., Ltd. (Shanghai, China). Total RNA was isolated from the mouse prefrontal cortex using Trizol reagent (Thermo Fisher, CA, USA) according to the manufacturer's protocol. The quantity and purity of RNA were assessed using the Bioanalyzer 2100 and RNA 6000 Nano LabChip Kit (Agilent, CA, USA), and only high-quality RNA samples with RNA integrity number (RIN) number > 7.0 were used for library construction.

After RNA extraction, mRNA was enriched from 5 μg of total RNA using Dynabeads Oligo (dT) (Thermo Fisher) through two rounds of purification. Subsequently, the mRNA was fragmented into short fragments at 94 °C for 5 to 7 min using a Magnesium RNA Fragmentation Module (NEB, Ipswich, MA, USA) and reverse-transcribed into cDNA using SuperScript™ II Reverse Transcriptase (Invitrogen). The synthesized cDNA was then converted into U-labeled second-stranded DNAs with E. coli DNA polymerase I (NEB), RNase H (NEB), and dUTP solution (Thermo Fisher). To prepare the DNA fragments for adapter ligation, an A-base was added to the blunt ends of each strand, followed by ligation to indexed adapter with T-base overhangs. Size selection of the ligated products was performed using AMPureXP beads. After treatment with heat-labile UDG enzyme (NEB) of the U-labeled second-strand DNAs, the ligated products underwent PCR amplification under the following conditions: initial denaturation at 95 °C for 3 min; 8 cycles of denaturation at 98 °C for 15 s, annealing at 60 °C for 15 s, and extension at 72 °C for 30 s; and a final extension at 72 °C for 5 min. The average insert size of the final cDNA libraries was 300 ± 50 bp. Finally, paired-end sequencing (PE150) with 2 × 150 bp reads was performed on an Illumina Novaseq™ 6000 platform following the vendor's recommended protocol.

Sequencing output comprises raw reads that may contain adapters or low-quality bases impacting subsequent assembly and analysis. To ensure high-quality clean reads, the data underwent further filtration using Cutadapt (version: cutadapt-1.9; https://cutadapt.readthedocs.io/en/stable/). Filtering criteria included: (1) removal of reads containing adapters; (2) elimination of reads with polyA and polyG sequences; (3) exclusion of reads with

over 5% unknown nucleotides (N); and (4) discarding low-quality reads containing more than 20% bases with a quality value of ≤ 20 (Q20). Sequence quality assessment was conducted using FastQC (version 0.11.9; http://www.bioinformatics.babraham.ac.uk/projects/fastqc/) to analyze parameters such as Q20, Q30, and GC-content of the resultant clean data. Subsequently, G gigabases of paired-end reads were obtained after cleaning. The raw sequence data will be submitted to the NCBI Gene Expression Omnibus (GEO) datasets, and the accession number will be provided upon successful upload.

Reads of all samples were aligned with the reference genome using the HISAT2 package (https://daehwankimlab.github.io/hisat2/, version: hisat2-2.2.1). Mapped reads from individual samples underwent assembly using StringTie (version: stringtie-2.1.6; http://ccb.jhu.edu/software/stringtie/) with default settings. Integration of transcriptomes from all samples facilitated the construction of a comprehensive transcriptome using gffcompare software (version: gffcompare-0.9.8; http://ccb.jhu.edu/software/stringtie/gffcompare.shtml). After transcriptome generation, StringTie and ballgown (http://www.bioconductor.org/packages/release/bioc/html/-ballgown.html) were used to estimate transcript expression levels and calculate Fragments Per Kilobase of transcript per Million mapped reads (FPKM) values for mRNA abundance analysis.

Bioinformatic analysis of RNA-seq data

Differential gene expression analysis was performed using DESeq2 software to compare two groups. When comparing two groups, genes with an average FPKM value of less than 1 in both groups were excluded from the analysis. Genes were considered DEGs based on p values < 0.05 and absolute fold change (FC) > 1.5. The volcano plots were generated using GraphPad Prism 9 (San Diego, CA, USA). The heat maps were produced online using BioLadder (https://www.bioladder.cn) based on differentially expressed genes by setting the criteria of p values < 0.05 or < 0.25. The principal component analysis (PCA) plots were created using the OmicStudio tools (https://www.omicstudio.cn). Gene Ontology (GO) enrichment analysis of DEGs was conducted using Metascape®, an online tool for gene function annotation analysis (https://metascape.org).

Quantitative real-time PCR

Total RNA was isolated from mouse prefrontal cortex tissues using Trizol reagent (Absin, Shanghai, China) and subjected to reverse transcription with the ReverTra Ace™ qPCR RT Master Mix (TOYOBO, Osaka, Japan). Quantitative real-time PCR was performed using the ChamQ Universal SYBR qPCR Master Mix (Vazyme, Shanghai, China) on the CFX96 Touch Real-Time PCR Detection System (Bio-rad, Hercules, CA, USA). The PCR protocol comprised an initial denaturation step at 95 °C for 30 s, followed by 50 cycles of denaturation at 95 °C for 30 s, annealing at 60 °C for 30 s, and extension at 95 °C for 15 s, with a final extension at 60 °C for 60 s. *Gapdh* was used as the endogenous control gene, and the relative mRNA expression levels were determined using the $2^{\exp(-\Delta\Delta Ct)}$ method. The primer sequences were synthesized by Sangon Biotech (Shanghai, China) and are listed in Additional file 1: Table S1.

BBB penetration prediction

The partition coefficient (cLogP) and acid dissociation constant (pKa) values for WRW4 and W peptide were estimated using ChemDraw software (version 20.0, PerkinElmer, Waltham, MA, USA).

Transcriptome datasets from brain tissues and blood samples of MDD or loneliness individuals

To investigate the gene expression of *FPR2* and its endogenous ligand *ANXA1* in MDD and loneliness, we conducted a comprehensive screening of brain tissue and peripheral blood datasets from the National Center for Biotechnology Information (NCBI) Gene Expression Omnibus (GEO) database (https://www.ncbi.nlm.nih.gov/geo/). The search query utilized was: "Major depression or Major depressive disorder or MDD or Loneliness or Lonely or Social isolation" AND "brain or blood" AND "Homo sapiens". Inclusion criteria comprised studies with patients with MDD or loneliness and healthy controls, samples from either brain or peripheral blood, and microarray or RNA sequencing technology. A total of 14 brain datasets (accession numbers: GSE54575, GSE54568, GSE54570, GSE54567, GSE12654, GSE53987, GSE54563, GSE54565, GSE54572, GSE54562, GSE54571, GSE54593, GSE54566, and GSE54564) and 5 peripheral blood cell datasets (GSE98793, GSE32280, GSE76826, GSE38206, GSE39653) of MDD were included. A total of 8 blood datasets (GSE68526, GSE7148, GSE25837, GSE65403, GSE65341, GSE65317, GSE65298, and GSE65213) of loneliness were included. Detailed characteristics of these datasets are provided in Additional file 1: Table S2–4.

Bioinformatics analysis of transcriptome datasets in the GEO database

The transcriptional expression of *FPR2* and *ANXA1* was analyzed using standardized quantile-normalized values provided by the corresponding datasets of brain tissues and/or blood samples. The GEO2R interactive network tool was utilized to identify the DEGs and fold change (FC) values of different transcriptome datasets [54]. The heat maps were performed online using BioLadder. GO analysis of DEGs from GSE38206 (with criteria: q

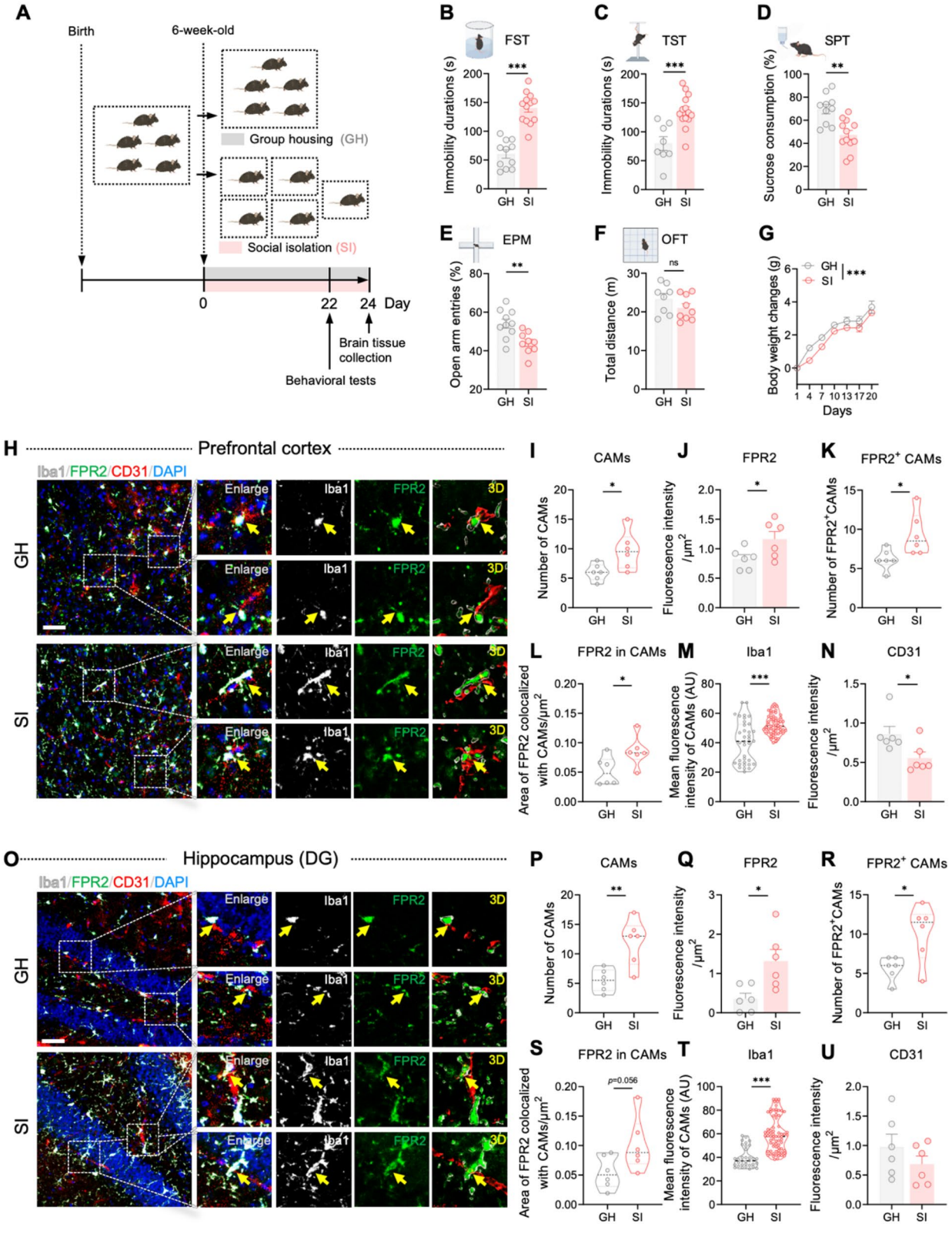

Fig. 1 (See legend on next page.)

(See figure on previous page.)

Fig. 1 Social isolation induces depressive and anxiety-like behaviors in mice and increases CAM activation and FPR2 expression in the mouse brains. **A**. Schematic representation of constructing a mouse model for social isolation-induced depression. **B**, **C**. SI mice exhibited increased immobility time in the forced swim test (FST) and the tail suspension test (TST) compared to GH mice. **D**. SI mice showed reduced sucrose consumption in the sucrose preference test (SPT) compared to GH mice. **E**. In the elevated plus maze (EPM) test, SI mice made fewer entries into the open arms. **F**. The open field test (OFT) showed no significant difference in total movement distance between SI and GH mice. **G**. SI mice displayed lower body weight compared to GH mice. Results are expressed as mean ± SEM, with 8–14 mice per group. Immunofluorescence staining was performed to assess CAM activation and FPR2 expression in the PFC (**H**) and the hippocampal DG region (**O**) of mice. Serial sections were stained for microglia using a rabbit anti-Iba1 antibody and Alexa Fluor 488-conjugated anti-rabbit IgG (white), and for CD31 using a rat anti-CD31 antibody followed by Alexa Fluor 555-conjugated anti-rat IgG (red). Subsequently, the sections were stained with a rabbit anti-FPR2 antibody conjugated with AF647 (green). Cell nuclei were counterstained with DAPI (blue). Scale bar, 50 μm. Selected areas are magnified 5.6 times and presented as composite images, individual fluorescence stains, and 3D reconstructed images generated by Imaris. The yellow arrow highlights CAMs whose cell bodies and/or processes directly interact with blood vessels. Quantitative analyses of the number of CAMs, the fluorescence intensity of FPR2, and the count of FPR2-positive CAMs in the PFC and hippocampal DG region are presented in panels (**I**, **P**), (**J**, **Q**), and (**K**, **R**), respectively. Additionally, the quantification of the area of FPR2 colocalized with CAMs, along with the fluorescence intensities of Iba1 and CD31 in the PFC and hippocampal DG region, are shown in panels (**L**, **S**), (**M**, **T**), and (**N**, **U**), respectively. Results are expressed as mean ± SEM, based on two individual fields for each region, using three mice per group. * $p < 0.05$, ** $p < 0.01$, *** $p < 0.001$. GH, group-housed; SI, socially isolated; CAMs, capillary-associated microglia; PFC, prefrontal cortex; DG, dentate gyrus

values < 0.05 and absolute FC > 1.5) and GSE54575 (with criteria: p values < 0.05 and absolute FC > 1.2) was conducted using Metascape®. The Gene Set Enrichment Analysis (GSEA) was performed using the OmicStudio tool.

Statistical analyses

All data are expressed as means ± SEM. Two-group comparisons were assessed using the two-tailed student's t-test. Multiple comparisons were performed using one-way ANOVA, followed by Tukey's post hoc test. The body weight of the mice was analyzed using two-way ANOVA. Spearman's correlation coefficient was used to assess the relationship between the fluorescence intensity of microglia (Iba1) and that of FPR2. All analyses were conducted using GraphPad Prism 9. A p-value of less than 0.05 was considered statistically significant.

Results

FPR2 in capillary-associated microglia increases in the social isolation model mice

To explore the involvement and mechanism of FPR2 in depression induced by social isolation, we housed 6-week-old C57BL/6J mice individually in cages for three weeks to establish a mouse model of social isolation (Fig. 1A). This model is widely used in studies of social isolation stress with minimal handling and non-invasive procedures [55]. It reflects current societal patterns of social isolation and serves as an ideal model for studying anxiety and related disorders, such as depression [55]. The depression-like behaviors of mice were evaluated by assessing immobility duration in the forced swim test (FST) and tail suspension test (TST), as well as their preference for sugar solution in the sucrose preference test (SPT). Anxiety-like behaviors were determined by quantifying the percentage of open-arm entries in the elevated plus maze (EPM) test. Spontaneous locomotor and exploratory activity were measured by recording the total distance traveled in the open field test (OFT). Compared to group-housed (GH) mice, individually housed (SI) mice exhibited significantly increased immobility in the FST and TST, reduced sugar preference in SPT, and decreased open-arm entries in the EPM (Fig. 1B–E). These results validate the successful establishment of a social isolation model that induces depressive and anxiety-like behaviors. In addition, SI and GH mice exhibited comparable distance traveled in the OFT (Fig. 1F), excluding the impact of locomotor and exploratory activity on depressive and anxiety-like behaviors. Body weight changes were also monitored in SI mice, revealing a slight reduction compared to GH mice (Fig. 1G).

Studies have demonstrated that microglial activation and BBB disruption are involved in the pathogenesis of depression, and there are direct contacts and interactions between capillary-associated microglia (CAMs) and cerebral blood vessels [29, 56]. FPR2 is expressed in microglia and is upregulated under certain pathological conditions [57]. This study utilized immunofluorescence staining to investigate changes in CAMs and FPR2 expression in the brains of SI mice. We defined CAMs as microglia whose cell bodies and/or processes are in contact with blood vessels, as indicated by the yellow arrows in Fig. 1H, O. Compared to GH mice, the number of cells colocalizing the microglial marker Iba1 and the endothelial cell marker CD31 was significantly increased in the prefrontal cortex (PFC) and the dentate gyrus (DG), cornu ammonis-1 (CA1), and cornu ammonis-3 (CA3) regions of the hippocampus in SI mice (Fig. 1I, P, and Additional file 1: Figure S1B, I). Brain endothelial cells are crucial components of the BBB, essential for maintaining its integrity. This result indicates that social isolation leads to an increase in CAMs in the brains of mice. Additionally, the expression of FPR2 was significantly increased in the PFC and hippocampus of SI mice, and both the number of FPR2-expressing CAMs and the expression levels of FPR2 in these microglia were markedly elevated (Fig. 1J–L, Q–S, and Additional file 1: Figure S1C–E, J–L). FPR2 colocalized with Iba1 accounted for

approximately 66–77% of the total expression of FPR2 in the PFC and hippocampus of GH mice, with this proportion further increasing (74–83%) in the brains of SI mice (Additional file 1: Figure S1O). These results indicate that FPR2 is predominantly expressed in microglia, and social isolation enhances its expression in microglia. The fluorescence intensity of Iba1 in CAMs within the PFC and hippocampus of SI mice was significantly enhanced (Fig. 1M, T, and Additional file 1: Figure S1F, M), while the fluorescence intensity of CD31 was decreased or showed a downward trend (Fig. 1N, U, and Additional file 1: Figure S1G, N). All these findings indicate that social isolation induces the activation of CAMs and causes damage to brain endothelial cells, with FPR2 potentially playing a significant role.

FPR2 antagonist WRW4 ameliorates SI-induced depressive and anxiety-like behaviors

Therefore, we employed peripheral administration of FPR2 antagonists or agonists to investigate the impact of modulating FPR2 signaling on depressive and anxiety-like behaviors induced by social isolation. Peripheral drug administration offers significant advantages over central administration in terms of drug safety and convenience. On the 14th day of SI modeling, the mice were subjected to behavioral tests, including the FST, TST, and SPT. SI mice displayed increased immobility in the FST and TST, and a reduced preference for sucrose in the SPT compared to GH mice (Additional file 1: Figure S2A-C), indicating that SI mice exhibited depressive-like behavior by the 14th day of social isolation. The FPR2 antagonist WRW4 (1.5 mg/kg), the agonist Ac2-26 (0.5 mg/kg), or W peptide (1.5 mg/kg) was subcutaneously administered on days 15, 17, 19, and 21 during the establishment of the mouse SI model, behavioral tests performed on the 22nd day (Fig. 2A, and Additional file 1: Figure S3A). Administration of WRW4 significantly decreased the immobility duration of SI mice in the FST and TST, increased their preference for sucrose solution in the SPT, and upregulated the frequency of their entering the open arm in the EPM (Fig. 2B–E). However, treatments with Ac2-26 or W peptide did not significantly affect immobility duration or sucrose preference in SI mice (Fig. 2B–D, and Additional file 1: Figure S3B–D). Ac2-26 treatment increased the tendency of SI mice entering the open arm in the EPM (Fig. 2E), while the W peptide did not (Additional file 1: Figure S3E). Furthermore, treatment with WRW4 or Ac2-26 showed no significant effect on the distance traveled by SI mice in the OFT (Fig. 2F). WRW4 and W peptide had no effect on SI-induced weight loss in mice (Additional file 1: Figure S4). These findings highlight that peripheral pharmacological inhibition of FPR2 can ameliorate SI-induced depressive and anxiety-like behaviors in mice.

WRW4 reduces SI-induced CAM activation and FPR2 expression in CAMs

We initially investigated the effect of WRW4 treatment on the overall activation of microglia in the brains of SI mice. Western blotting revealed a significant increase in the expression of Iba1 in the PFC of SI mice compared to the GH group (Fig. 3A, B), indicating the overall activation of microglia induced by social isolation. Treatment with WRW4 peripherally effectively suppressed social isolation-induced microglial activation (Fig. 3A, B). Immunofluorescence staining further validated the reduction of microglial activation in the PFC and hippocampus of SI mice with WRW4 treatment. WRW4 inhibited the increase in Iba1 expression and the enlargement of microglial somas in these brain regions of SI mice (Fig. 3D–F). Astrocytes are the most abundant type of glial cells in the brain and also contribute to immune responses. Classically activated microglia can induce the activation of astrocytes termed A1 astrocytes [58]. Interestingly, consistent with the findings reported by Cheng et al. [59], we did not observe a significant effect of social isolation on the expression of the glial fibrillary acidic protein (GFAP, a marker of astrocyte activation) in the PFC of SI mice (Fig. 3A, C). The expression of GFAP in the hippocampal DG and CA1 regions showed a tendency to increase (Additional file 1: Figure S5A, B). Moreover, WRW4 treatment significantly reduced GFAP expression in the CA1 region of SI mice (Additional file 1: Figure S5A, B). These findings suggest that peripheral WRW4 administration alleviates the activation of microglia and astrocytes in the brains of SI mice.

Then, we verified whether WRW4 treatment could reverse the activation of CAMs and increased FPR2 expression caused by social isolation. As expected, WRW4 treatment significantly reduced the number of CAMs and the expression of FPR2 in the PFC and hippocampus of SI mouse brains (Fig. 4A–C, H–J, and Additional file 1: Figure S6A–C, H–J). WRW4 treatment also decreased the FPR2-expressing CAMs and FPR2 expression within these microglia in the brains of SI mice (Fig. 4D, E, K, L, and Additional file 1: Figure S6D, E, K, L). The Iba1 in CAMs of SI mouse brains was reduced, while the fluorescence intensity of CD31 was enhanced in the PFC (Fig. 4F, G, M, N, and Additional file 1: Figure S6F, G, M, N). Furthermore, the fluorescence intensity of Iba1 was positively correlated with FPR2 expression in the PFC and hippocampus of GH, SI, and SI + WRW4 mice (Additional file 1: Figure S7A–D). All these findings suggest that FPR2 inhibition reverses the activation of CAMs and brain endothelial cell damage induced by social isolation.

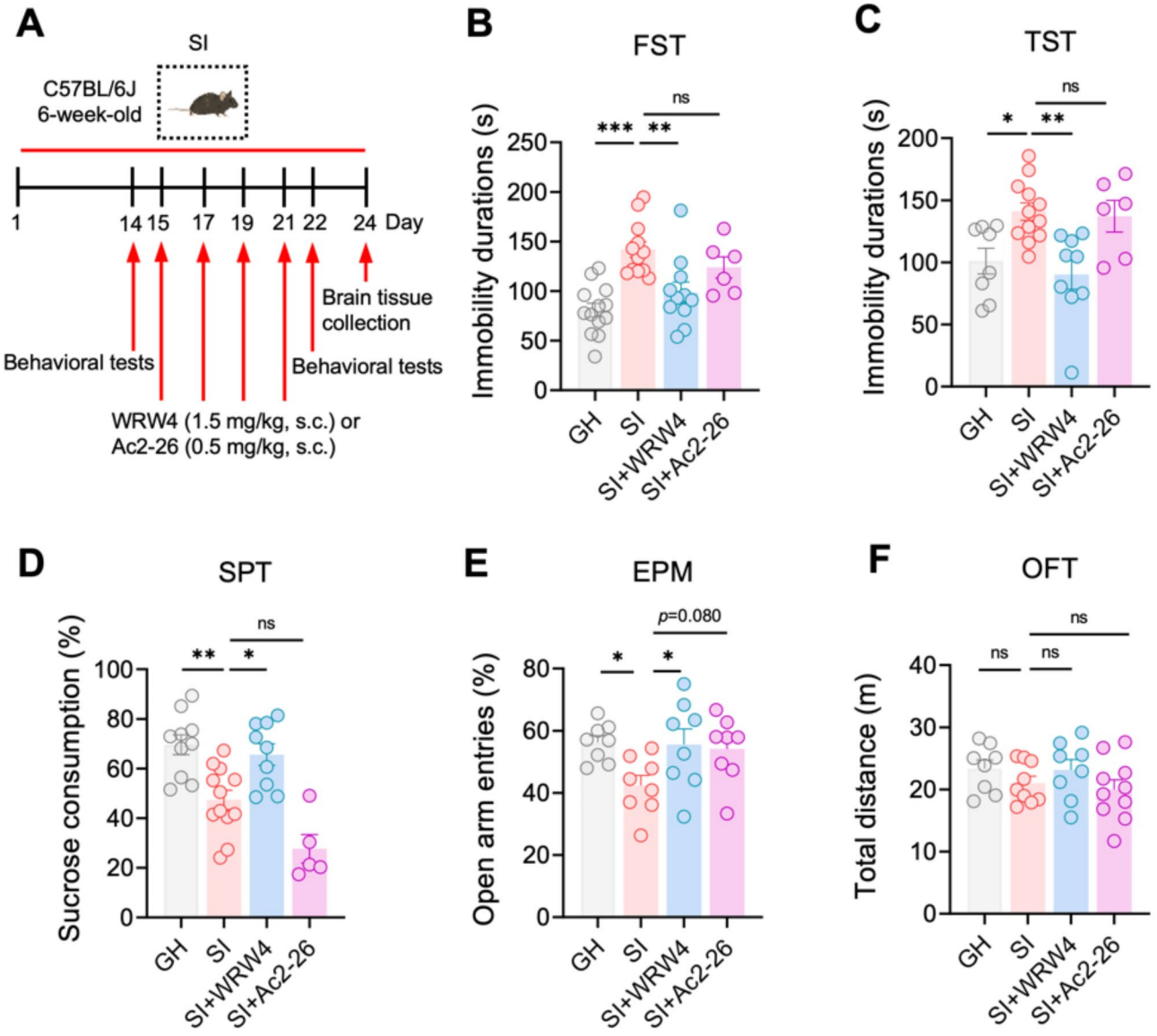

Fig. 2 Inhibition of FPR2 alleviates depressive and anxiety-like behaviors in mice subjected to social isolation. **A.** Schematic representation of the experimental procedure for the subcutaneous administration of WRW4 or Ac2-26 to the social isolation model mice. **B**, **C.** Administration of WRW4, but not Ac2-26, decreased immobility time in the forced swim test (FST) and the tail suspension test (TST) in SI mice. **D.** Administration of WRW4, but not Ac2-26, increased the percentage of sucrose uptake in the sucrose preference test (SPT) in SI mice. **E.** WRW4 increased the percentage of SI mice entering the open arms of the elevated plus maze (EPM) test. **F.** Neither WRW4 nor Ac2-26 affected the total movement distance of SI mice in the open field test (OFT). Results are expressed as mean ± SEM, with 5–13 mice per group. * $p < 0.05$, ** $p < 0.01$, *** $p < 0.001$. GH, group-housed; SI, socially isolated; s.c., subcutaneous

WRW4 alleviates SI-induced neuronal damage

We further investigated the impact of WRW4 treatment on neuronal damage induced by social isolation, including neuronal loss and synaptic disruption. Nissl staining revealed a notable reduction in the number of neurons in the PFC and hippocampus due to social isolation (Fig. 5A, B), along with neuronal morphological changes resembling dark neurons [60], including cell body shrinkage, nuclear pyknosis, chromatin condensation, or abnormal basophilia (Fig. 5A). Peripheral WRW4 treatment effectively reversed the decrease in neuronal density and increase in dark neurons induced by social isolation (Fig. 5A-C). Furthermore, compared with GH mice, a marked reduction of SYN (synaptophysin, a presynaptic marker) and post-synaptic density 95 (PSD95, a post-synaptic marker) was observed in the PFC of SI mice by Western blots (Fig. 5D–F). Consistent with the findings of Western blots, immunofluorescence staining also demonstrated downregulation of SYN expression in the PFC and hippocampal DG, CA1, and CA3 regions of

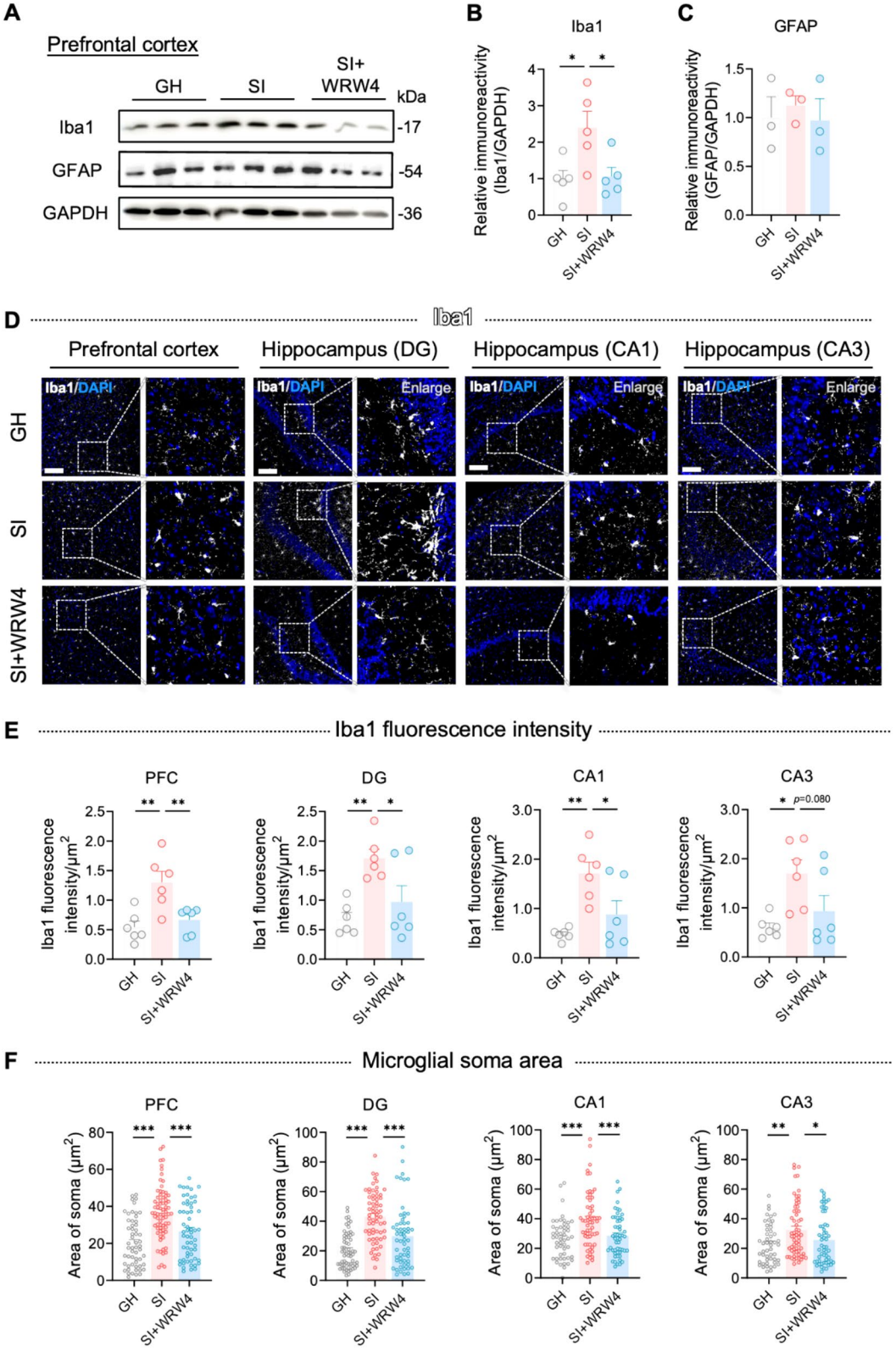

Fig. 3 (See legend on next page.)

(See figure on previous page.)

Fig. 3 WRW4 treatment reduces microglial activation induced by social isolation in the PFC and hippocampus of SI mice. **A.** Representative images of Western blot analysis demonstrating the expression of Iba1 and GFAP in the PFC of GH mice, SI mice, and SI mice treated with WRW4. **B**, **C.** Quantification of blot immunoreactivity normalized to GAPDH. **D.** Immunofluorescence staining was conducted to evaluate microglial activation in the PFC and the DG, CA1, and CA3 regions of the hippocampus in the mouse brain. Serial sections from mice were stained for microglia using a rabbit anti-Iba1 antibody and Alexa Fluor 488-conjugated anti-rabbit IgG (white). Nuclei were counterstained with DAPI (blue). Scale bar, 100 μm. Selected areas are magnified 11.4 times. Quantification of Iba1 fluorescence intensity (**E**) and microglial soma area (**F**) in the PFC and hippocampal DG, CA1, and CA3 regions are shown. Results are expressed as the mean ± SEM, based on two individual fields for each region (**E**) or 18–25 cells for each region (**F**), using three mice per group. * $p < 0.05$, ** $p < 0.01$, *** $p < 0.001$. GH, group-housed; SI, socially isolated; PFC, prefrontal cortex; DG, dentate gyrus; CA1, cornu ammonis-1; CA3, cornu ammonis-3

SI mice (Fig. 5G, H). WRW4 treatment restored the levels of these two synaptic proteins in socially isolated mice (Fig. 5D–H). These findings indicate that inhibiting FPR2 alleviates neuronal loss and synaptic damage caused by social isolation.

SI-induced transcriptomic changes in the PFC of mice

To elucidate the molecular mechanisms by which FPR2 mitigates behavioral and histological phenotypes in SI mice, we characterized the transcriptome of the mouse PFC using RNA-seq (Fig. 6A). Initially, we compared RNA-seq data from SI mice and GH mice, identifying 137 differentially expressed genes (DEGs), 70 upregulated and 67 downregulated in SI versus GH (absolute fold change [FC] > 1.50, $p < 0.05$), along with a distinct transcriptional signature for the PFC in SI mice (Fig. 6B, Additional file 1: Figure S8, and Additional file 2: Table S5). Gene Ontology (GO) analysis of these DEGs revealed that at least half of the top 15 biological processes (BP), molecular functions (MF), and cellular components (CC) involved in ion channels, transport, adhesion, extracellular matrix, and endothelial cells, which are related to the function of BBB (Fig. 6C). Most of the DEGs in these enriched GO categories exhibited downregulated (Fig. 6C). Therefore, we conducted a comprehensive analysis of the changes in genes specifically expressed in brain endothelial cells [61, 62]. Compared to GH mice, 23 brain endothelial cell-specific expression genes were altered in the PFC of SI mice, including transporter (such as *Slc29a4*, $p < 0.001$, Fig. 6B, D, E) and tight junction genes, all of which were downregulated (Fig. 6D, $p < 0.25$, an asterisk indicates $p < 0.10$). Moreover, similar to other neurological disorder model mice (including stroke, MS, TBI, or seizure) [61], the gene expression profile of brain endothelial cells in SI mice shifts to a peripheral endothelial cell-like state, characterized by the upregulation of specific genes (Fig. 6D, $p < 0.25$, an asterisk indicates $p < 0.10$). We further compared the single-nucleus sequencing database from the PFC of MDD patients published by Nagy et al. Their study identified a total of 41 DEGs (FDR < 0.10) across 16 cell clusters when compared to healthy controls [63]. Notably, thirteen of these DEGs in the PFC of MDD patients also exhibited changes in the corresponding brain region of the SI mice in this study, including the brain endothelial-specific genes *Zfp36* and *Grin2a* (Fig. 6F, $p < 0.25$, an asterisk indicates $p < 0.10$).

Additionally, GO analysis also showed that functions related to hormone activity (including DEGs such as *Agt*, *Trh*, and *Pthlh*) and T cell activation (*Spi1*, *Psgs*, and *Ceacams*) were also enriched in the brains of SI mice, indicating dysfunction of the HPT axis and immune response (Fig. 6B, C, E). The top-ranked DEGs also include *Hnrnpa3* ($p = 1.25 \times 10^{-197}$) and *Camk2d* ($p = 1.61 \times 10^{-5}$), which are predominantly expressed in neurons [64], *Zbtb20* ($p = 2.77 \times 10^{-9}$), which is highly expressed in astrocytes [65], and *Pcdhs*, which are expressed in both cell types and brain endothelial cells [66] (Fig. 6B, G). The HNRNPA3 encoded by *Hnrnpa3* participates in mRNA transport and splicing [67]. It is reduced in the brains of patients with early-stage AD [68]. In this study, the transcription level of *Hnrnpa3* in the PFC of SI mice was only 5.8% of that observed in GH mice, indicating a 17-fold reduction in mRNA levels (Fig. 6B, and Additional file 2: Table S5). RT-qPCR was used to validate the transcription levels of *Hnrnpa3. T*he results were consistent with the RNA-seq findings (Fig. 6E). ZBTB20, a transcriptional repressor, was found to be upregulated, while calcium/calmodulin-dependent protein kinase II delta (CAMK2D), which mediates calcium-dependent signaling, showed downregulation in the PFC of SI mice (Fig. 6B, and Additional file 2: Table S5). These two DEGs have been implicated in cognitive function and neurodevelopment [69, 70]. They overlapped with SFARI autism spectrum disorders (ASD) genes [71], which are associated with autism susceptibility. Additionally, two other *Camks*, *Camk2n2* and *Camk1d*, which were found to be altered in MDD patients, also showed changes in the SI mice of this study. Protocadherins (PCDHs), encoded by *Pcdhs*, are cell adhesion molecules that belong to the cadherin superfamily and play crucial roles in neuronal survival, dendritic self-avoidance (recognition), and synaptic development [72–75]. Compared to GH mice, more than 25% of *Pcdh* genes were altered in the PFC of SI mice ($p < 0.10$, 17 out of 59 genes), including seven DEGs such as *Pcdha6*, $p = 3.35 \times 10^{-17}$, *Pcdhgb1*, $p = 3.19 \times 10^{-8}$, and *Pcdhga8*, $p = 1.80 \times 10^{-4}$) (Fig. 6B, E, G, and Additional file 2: Table S5). Studies indicate that PCDHA6 may contribute to the pathogenesis of MDD [76].

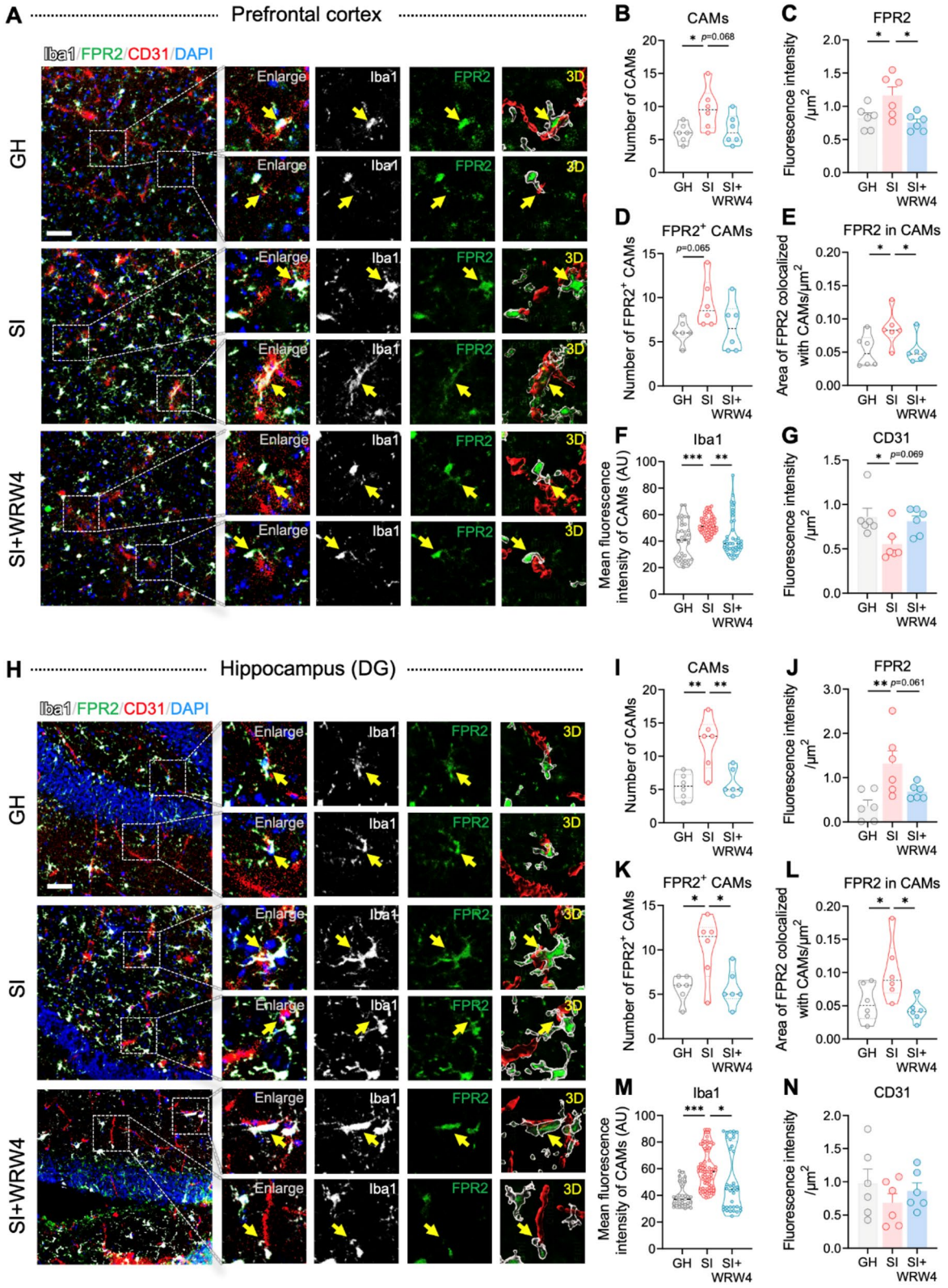

Fig. 4 (See legend on next page.)

(See figure on previous page.)

Fig. 4 WRW4 treatment reverses increased activation of CAMs and FPR2 expression in the PFC and hippocampal DG region in SI mice. Immunofluorescence staining was performed to assess CAM activation and FPR2 expression in the PFC (**A**) and the hippocampal DG region (**H**) of GH, SI, and WRW4-treated SI mice. Serial sections were stained for microglia using a rabbit anti-Iba1 antibody and Alexa Fluor 488-conjugated anti-rabbit IgG (white), and for CD31 using a rat anti-CD31 antibody followed by Alexa Fluor 555-conjugated anti-rat IgG (red). Subsequently, the sections were stained with a rabbit anti-FPR2 antibody conjugated with AF647 (green). Cell nuclei were counterstained with DAPI (blue). Scale bar, 50 μm. Selected areas are magnified 5.6 times and presented as composite images, individual fluorescence stains, and 3D reconstructed images generated by Imaris. The yellow arrow highlights CAMs whose cell bodies and/or processes directly interact with blood vessels. Quantitative analyses of the number of CAMs, the fluorescence intensity of FPR2, and the count of FPR2-positive CAMs in the PFC are presented in panels (**B**), (**C**), and (**D**), respectively. Additionally, the quantification of the area of FPR2 colocalized with CAMs, along with the fluorescence intensities of Iba1 and CD31 in the PFC, are shown in panels (**E**), (**F**), and (**G**), respectively. For the DG region of the hippocampus, the quantification of the number of CAMs, the fluorescence intensity of FPR2, and the number of FPR2-positive CAMs are presented in panels (**I**), (**J**), and (**K**), respectively. The quantification of the area of FPR2 colocalized with CAMs, as well as the fluorescence intensity of Iba1 and CD31, are shown in panels (**L**), (**M**), and (**N**), respectively. Results are expressed as mean ± SEM, based on two individual fields for each region, using three mice per group. * $p < 0.05$, ** $p < 0.01$, *** $p < 0.001$. GH, group-housed; SI, socially isolated; CAMs, capillary-associated microglia; PFC, prefrontal cortex; DG, dentate gyrus

Additionally, another top-ranked DEG, *Spp1* (also known as osteopontin), a marker gene for immature and disease-associated microglia (DAM), demonstrated a significant decrease in the PFC of SI mice (Fig. 6B, and Additional file 2: Table S5). SPP1 is downregulated in the microglia of LPS-induced depressed mice [77] and in the serum of MDD patients [78]. These results suggest that social isolation induces alterations in brain homeostasis in mice, including BBB dysfunction, dysregulated immune response, and pathological neuronal damage.

WRW4 partially reverses SI-induced transcriptomic changes in PFC

We then investigated the effect of peripheral treatment with the FPR2 inhibitor WRW4 on the transcriptome of SI mouse PFC. Compared to SI model mice, 191 DEGs, 109 upregulated and 82 downregulated, were identified in the PFC of SI mice treated with WRW4 (Fig. 6H, and Additional file 3: Table S6). Notably, 33% of upregulated DEGs (23 genes) and 33% of downregulated DEGs (22 genes) in SI mice versus GH mice were reversed by peripheral WRW4 treatment (Fig. 6I, J). Analysis of DEGs by principal component analysis (PCA) found that the transcriptome signature of the PFC of SI mice after WRW4 treatment was close to that of GH mice. The PFC transcriptome profile of SI mice was significantly different from these two groups of mice (Fig. 6K). GO analysis of DEGs revealed that eight of the top 15 BP, MF, and CC are related to ion channels, transport, and endothelial cells, and most of the DEGs in enriched GO categories showed upregulated (Fig. 6L). Many DEGs mentioned above between SI mice and GH mice, such as *Slc29a4*, *Agt*, *Hnrnpa3*, and *Pcdha6*, were reversed after WRW4 treatment (Fig. 6E, J). Moreover, the WRW4 treatment reversed the SI-induced downregulation of numerous brain endothelial-specific genes and alleviated the transition of brain endothelial cells to a peripheral endothelial cell-like state (Fig. 6M). WRW4 ameliorated changes in various genes associated with MDD and the *Pcdh* gene family (Fig. 6N, O).

Given the crucial roles of SLC29A4 and PCDHA6 in physiological and pathological processes in the brain, in addition to employing RT-qPCR to validate their altered expression profiles observed in RNA-seq, we also utilized western blot analysis and immunofluorescence staining to verify the changes in their protein expression levels and the cell types in which they are expressed. Consistent with the changes in transcription levels, the protein expression of SLC29A4 and PCDHA6 were significantly reduced in the PFC and hippocampus of SI mice compared to GH mice. Notably, treatment with WRW4 upregulated their expression in the SI mice (Fig. 7A–K, and Additional file 1: Figure S9A–D). Immunofluorescence staining revealed that SLC29A4 was primarily expressed in brain endothelial cells (Fig. 7D–G). However, PCDHA6 is mainly expressed on neurons according to the staining patterns, with a minor punctate distribution observed in brain endothelial cells (Fig. 7H–K). These results confirmed the phenomena observed in our RNA-seq data, suggesting that SI induces damage to the BBB and neuronal functions in the mouse brain, and inhibiting FPR2 can alleviate these pathological damages.

WRW4 alleviates SI-induced impairment of BBB integrity

The above results have demonstrated that peripheral inhibition of FPR2 largely reversed the altered expression profiles of BBB-related and neuronal function-associated molecules within the mouse brain induced by social isolation. The integrity of the BBB is crucial for maintaining the homeostasis of physiological functions in the brain. We speculate that the mechanism by which inhibiting FPR2 improves depressive and anxiety-like behaviors in mice may be related to its protection of the BBB. We assessed BBB's integrity by investigating albumin's permeability into the CNS. As shown in Fig. 8A–E, albumin levels in the PFC and DG, CA1, and CA3 regions of the hippocampus from SI mice were significantly increased, and albumin co-localized with CD31 and entered the brain parenchyma elevated compared with GH mice (Fig. 8A–D, F). This result suggests that social isolation damages the BBB integrity of mice. Notably, peripheral

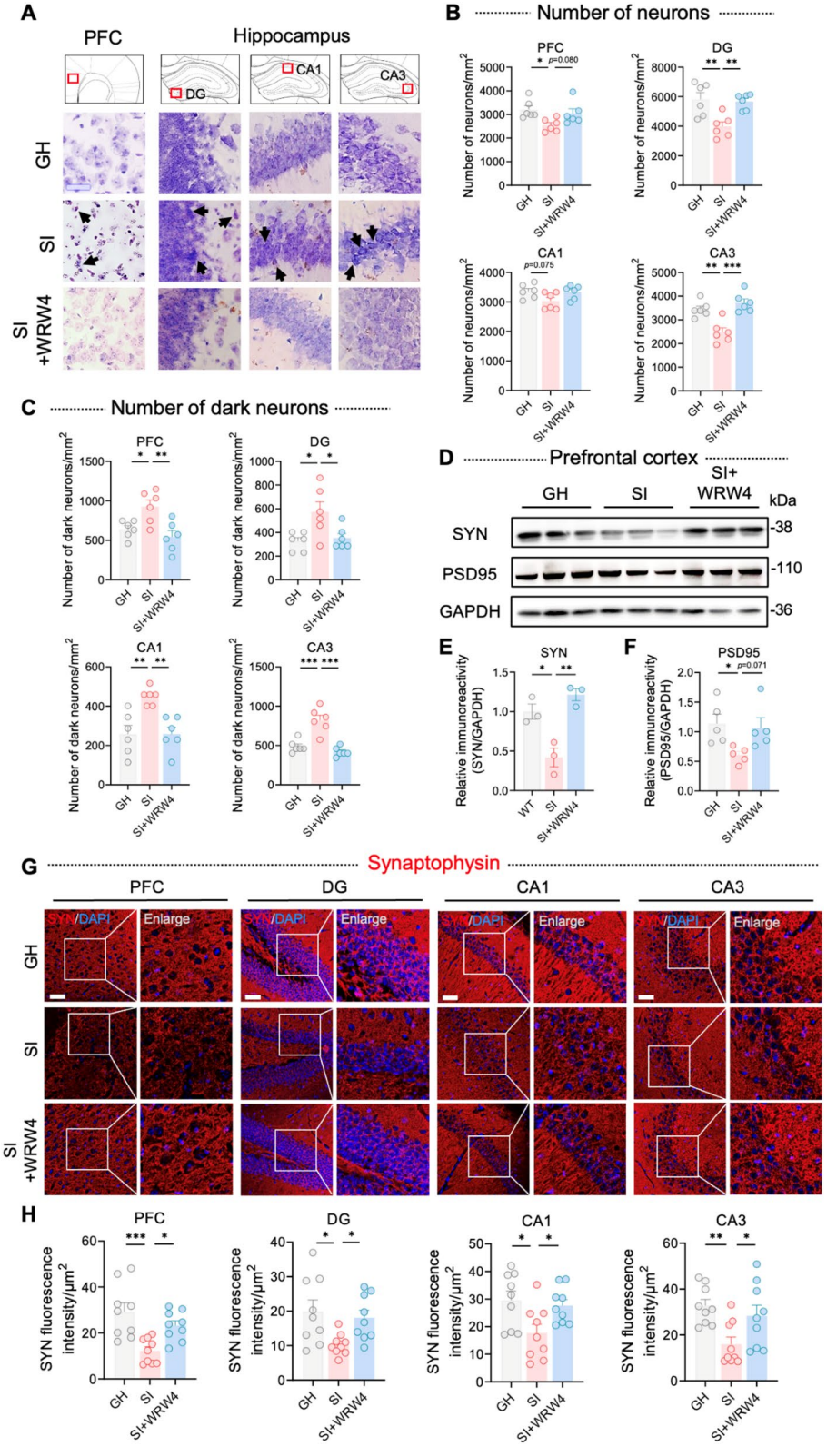

Fig. 5 (See legend on next page.)

(See figure on previous page.)

Fig. 5 WRW4 treatment alleviates the neuron loss and synaptic damage induced by social isolation in the PFC and hippocampus of SI mice. **(A)** Nissl staining was performed to assess neuronal damage in the PFC and hippocampal DG, CA1, and CA3 regions of GH, SI, and WRW4-treated SI mice. Serial sections were stained for Nissl bodies using a Nissl staining solution as described in the "Methods" section. The black arrows indicate the dark neurons. Scale bar, 30 μm. **(B)** Quantification of the number of Nissl body-positive cells in the PFC and hippocampus. **(C)** Quantification of the number of dark neurons in the PFC and hippocampal DG, CA1, and CA3 regions of the mice. **(D)** Representative images of Western blot analysis showing the expression of SYN and PSD95 in the PFC of the mice. **E**, **F.** Quantification of immunoreactivity of the blots normalized to GAPDH. **G.** Immunofluorescence staining was conducted to evaluate pre-synaptic damage in the PFC and hippocampal DG, CA1, CA3 regions in the mouse brain. Serial sections from mice were stained for SYN using a rabbit anti-synaptophysin antibody and Alexa Fluor 647-conjugated anti-rabbit IgG (red). Nuclei were counterstained with DAPI (blue). Scale bar, 50 μm. **H.** Quantification of SYN fluorescence intensity in PFC and hippocampal DG, CA1, and CA3 regions. Results are expressed as the mean ± SEM, based on two or three individual fields for each region, using three mice per group. * $p < 0.05$, ** $p < 0.01$, *** $p < 0.001$. GH, group-housed; SI, socially isolated; PFC, prefrontal cortex; DG, dentate gyrus; CA1, cornu ammonis-1; CA3, cornu ammonis-3; SYN, synaptophysin

administration of WRW4 markedly attenuated the leakage of peripheral albumin into the brain parenchyma in these regions in SI mice. In addition, WRW4 also reduced albumin penetration into cortical areas and the entorhinal cortex parenchyma of SI mice (Additional file 1: Figure S10A–D). These findings indicate a potential role for peripheral FPR2 inhibition in mitigating social isolation-induced impairment of BBB permeability.

In addition, the ability of the synthetic peptide ligands WRW4 and W peptide to penetrate the BBB was predicted using ChemDraw. According to the reports, a molecule is more likely to cross the BBB if its partition coefficient (cLogP) falls between 2.0 and 4.0, and its acid dissociation constant (pKa) ranges between 6.0 and 10.5. The cLogP and pKa values for WRW4 are 2.52 and 7.14, respectively, while the W peptide has values of 0.23 for cLogP and 7.15 (9.40 or 10.00) for pKa (Additional file 1: Figure S11). These results suggest that WRW4 may possess the capability to cross the BBB. We further verified the impact of direct intracerebral administration of WRW4 on depressive and anxiety-like behaviors in SI mice. The WRW4 (5 μg per mouse) was administered via intracerebroventricular (ICV) on the 18th day after establishing the SI mouse model, with behavioral tests performed on the 21st day (Fig. 9A). This treatment decreased the immobility duration of SI mice in the FST and TST, increased their preference for sucrose solution in the SPT, and upregulated the frequency of entries into the open arm in the EPM (Fig. 9B–E). Furthermore, WRW4 treatment did not significantly affect the distance traveled by SI mice in the OFT (Fig. 9F). These findings confirmed that central pharmacological inhibition of FPR2 can ameliorate SI-induced depressive and anxiety-like behaviors in mice.

Upregulation of *FPR2* transcription in OvPFC and blood in MDD patients

FPR2 is a crucial molecule in central and peripheral innate immunity [34]. Since social isolation leads to elevated expression of FPR2 in CAMs, and peripheral inhibition of FPR2 can mitigate the depressive and anxiety-like behaviors induced by social isolation, we analyzed publicly available datasets from the NCBI GEO database to examine changes in *FPR2* transcription in the brain and peripheral blood cells of individuals with loneliness and/or major depressive disorder. Utilizing the keywords "Social isolation", "Loneliness", "Major depressive disorder", "Major depression", or "MDD" in conjunction with "brain" or "blood", we identified a total of eight brain tissue transcriptome datasets from individuals with loneliness, as well as 14 brain tissue transcriptome datasets and five peripheral blood cell transcriptome datasets from MDD patients (Additional file 1: Table S2–4). We did not find transcriptomic datasets from brain samples of patients with loneliness. Moreover, compared with healthy controls, the alterations in the transcriptional levels of *FPR2* and *ANXA1* in peripheral blood cells of individuals with loneliness were not readily apparent (Additional file 1: Figure S12). Intriguingly, among the five peripheral blood cell databases of MDD patients, the transcriptional levels of *FPR2* and *ANXA1* were simultaneously upregulated in two of these databases, GSE38206 and GSE76826 (Fig. 10A–E). These two databases recruited older MDD patients compared to the other databases (Additional file 1: Table S3). Additionally, the GSE38206 dataset used peripheral blood mononuclear cells (PBMCs) from MDD patients with high Hamilton depression rating scale (HDRS-17) scores who were experiencing a severe depressive episode (Additional file 1: Table S3). The transcription levels of *FPR2* were significantly elevated in PBMCs of MDD patients compared to healthy controls in this dataset (FC = 3.0, $p = 6.34 \times 10^{-4}$) (Fig. 10A, and Additional file 1: Table S3). Therefore, we further performed gene ontology (GO) term analysis and gene set enrichment analysis (GSEA) using this dataset.

GO term analysis of DEGs (absolute FC > 1.50, $q < 0.05$) revealed that at least half of the top 15 enriched GO terms linked to infection and immune responses were upregulated, such as cellular response to cytokine stimulus, positive regulation of cytokine production, leukocyte activation, and defense response to virus (Fig. 10D). GSEA analysis indicated the upregulation of the chemokine signaling pathway and T cell receptor signaling pathway in PBMCs from MDD patients compared to healthy controls (Fig. 10E). These findings indicate that increased expression of FPR2 may contribute to enhanced

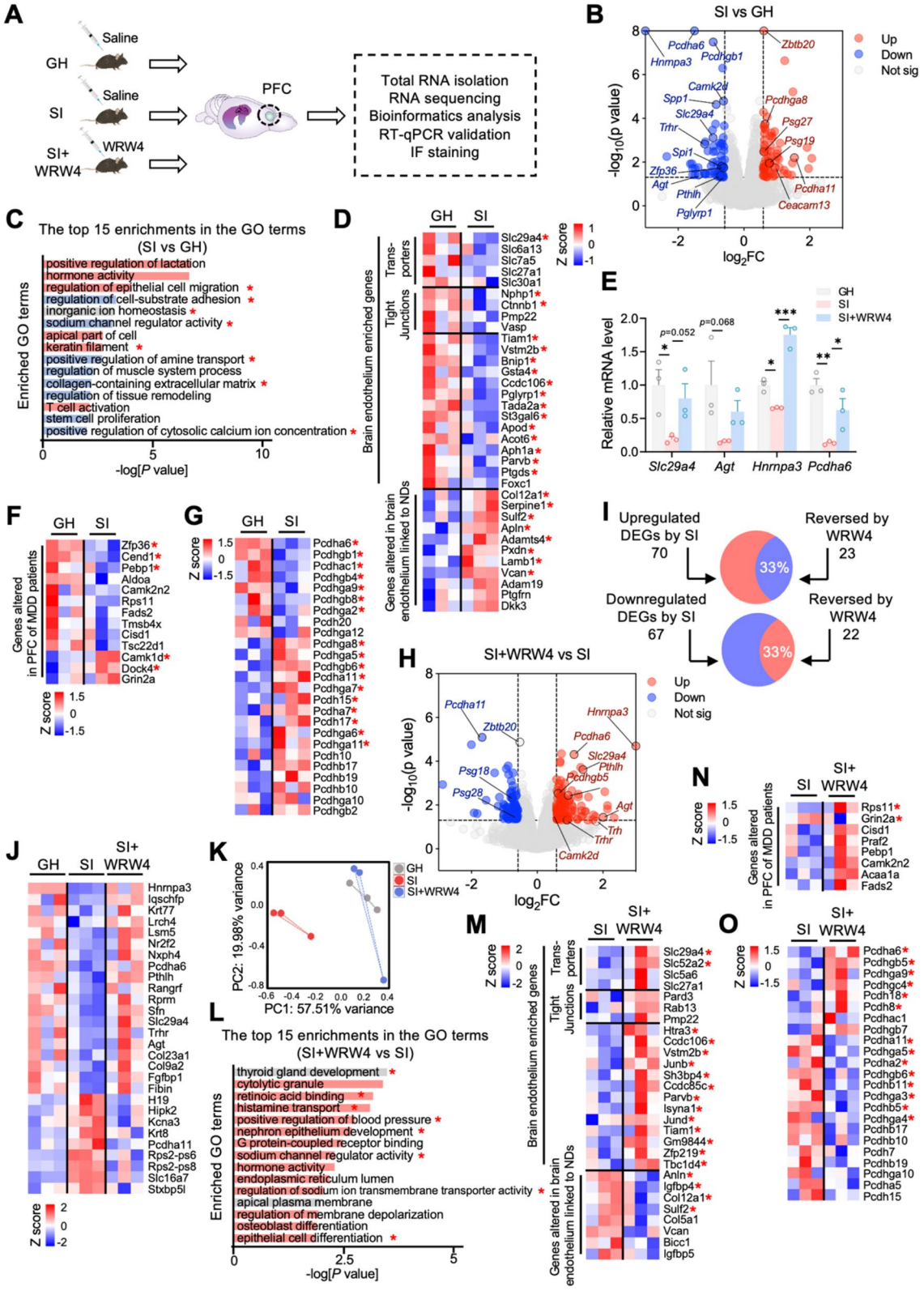

Fig. 6 (See legend on next page.)

(See figure on previous page.)

Fig. 6 WRW4 treatment reverses transcriptomic changes induced by social isolation in the PFC of SI mice. **(A)** Schematic diagram illustrating the experimental workflow for RNA-seq and analysis. **(B)** Volcano plot depicting differentially expressed genes (DEGs, with absolute fold change [FC] > 1.50, $p < 0.05$) from the PFC of GH and SI mice. **(C)** Gene ontology (GO) analysis of DEGs from GH and SI mice, presenting the top 15 enriched differential regulated pathways ranked by *p*-value, with asterisks indicating categories related to the BBB function. **(D)** Heat map showing changes in brain endothelium-enriched genes and endothelial cell genes associated with neurological disorders (NDs) in SI mice compared to GH mice. **(E)** RT-qPCR was used to verify the transcript levels of *Slc29a4*, *Agt*, *Hnrnpa3*, and *Pcdha6* in the PFC of the mice. **(F)** Heat map of alterations in MDD-related genes in SI mice compared to GH mice. **(G)** Heat map illustrating changes of *Pcdh* genes in SI mice compared to GH mice. **(H)** Volcano plot depicting DEGs (absolute FC > 1.50, $p < 0.05$) from WRW4-treated and untreated SI mice. **(I)** Venn diagram displaying 137 DEGs (70 upregulated and 67 downregulated, absolute FC > 1.50, $p < 0.05$) in SI mice compared to GH mice. WRW4 treatment reversed the expression of 23 upregulated DEGs and 22 downregulated DEGs in SI mice, with functionally annotated genes presented in a heat map (**J**). **K.** Principal component analysis (PCA) plot of these reversed genes from GH, SI, and WRW4-treated SI mice. **L.** GO analysis of DEGs from WRW4-treated and untreated SI mice, presenting the top 15 enriched differential regulated pathways ranked by *p*-value, with asterisks indicating categories related to the BBB function. **M.** Heat map illustrating changes in brain endothelium-enriched genes and endothelial cell genes related to NDs when comparing WRW4-treated and untreated SI mice. **N.** Heat map showing alterations in MDD-related genes in WRW4-treated and untreated SI mice. **O.** Heat map illustrating changes of *Pcdh* genes in WRW4-treated and untreated mice. The heat maps in panels **D**, **F**, **G**, and **M-O** display genes with *p*-values less than 0.25, with asterisks indicating *p*-values less than 0.10. GH, group-housed; SI, socially isolated; PFC, prefrontal cortex

inflammatory responses in the peripheral blood cells of patients with MDD.

We further analyzed the expression of *FPR2* in the brains of MDD patients. Sixteen brain tissue transcriptome databases were selected, which included various brain regions of MDD patients, such as the PFC, hippocampus (HIP), anterior cingulate cortex (ACC), amygdala (AMY), and associative striatum (AST) (Fig. 10F). Among them, in a dataset of orbital ventral PFC (ovPFC) region samples from MDD patients (GSE54575), *FPR2* and *ANXA1* transcript levels were increased or showed an upregulation trend, respectively, compared with healthy controls (Fig. 10F–H). Further enrichment analysis of GO terms found that more than half of the top 15 GO terms were related to protein synthesis or degradation, including RNA splicing (Fig. 10I). In this study, RNA-seq of PFC tissue in SI mice also found that the transcription of RNA splicing-related genes was dysregulated. In addition, changes in endothelial cell function in the ovPFC region of MDD patients were also observed. To verify the BBB damage in the brains of MDD patients, we performed GSEA on brain endothelial cell clusters in the sn-RNA seq database from the PFC tissue of MDD patients [63]. Consistent with the results of our SI model mice, most of the enriched top pathways in brain endothelial cells were downregulated compared to healthy controls (13 out of the top 15 enriched pathways were downregulated), including tight junction, adherens junction, focal adhesion, and regulation of actin cytoskeleton, which are closely related to endothelial function (Fig. 10J, K). These results suggest that FPR2 may have a potential role in specific brain regions with MDD patients. Moreover, BBB function is downregulated in MDD patients.

Discussion

Studies have reported microglial dysfunction and BBB damage in the brains of individuals with SI and depression, as well as in corresponding mouse models [79, 80]. A complex interaction exists between microglia and the BBB. CAMs, which are microglia in direct contact with cerebral blood vessels, have been less extensively studied concerning their effects on vascular function and their roles in psychiatric disorders. In this study, we identified for the first time an increase in the number of CAMs in the PFC and hippocampus of socially isolated mice. Notably, we observed that the expression of FPR2 in these CAMs is higher than in the group-housed mice. Peripheral administration of the FPR2 antagonist WRW4 reverses these changes and alleviates social isolation-induced depressive and anxiety-like behaviors in mice. We speculate that WRW4 likely possesses the ability to penetrate the BBB, as indicated by ChemDraw analysis. Furthermore, ICV injection of WRW4 also alleviates depressive and anxiety-like behaviors in SI mice. Analysis of public databases revealed that FPR2 is upregulated in the ovPFC tissue of individuals of MDD and the PBMCs of MDD patients during severe episodes. These findings suggest that the administration of FPR2 antagonists may inhibit FPR2 activation in brain CAMs, thereby alleviating depressive and anxiety-like behaviors in SI mice. FPR2 may represent a potential therapeutic target for depression induced by social isolation.

The mechanisms by which CAMs regulate vascular function remain not fully understood. Under physiological conditions, approximately 20–30% of microglia are in physical contact with blood vessels [27, 29]. Studies have shown that CAMs interact with vascular structures at locations not covered by astrocyte endfeet and can mobilize along the vessels [27]. Kisler et al. demonstrated that CAMs exhibit characteristics similar to those of parenchymal microglia, and their interactions with blood vessels are partially regulated by purinergic P2RY12 signaling. They also found that CAMs are crucial in regulating vascular tone and blood flow [29]. Additionally, Haruwaka et al. confirmed that microglia in the mouse brain migrate toward cerebral blood vessels during systemic inflammation. These migrating microglia initially help to maintain BBB integrity by expressing the tight-junction protein Claudin-5. However, with sustained inflammation, CAMs phagocytose astrocytes endfeet,

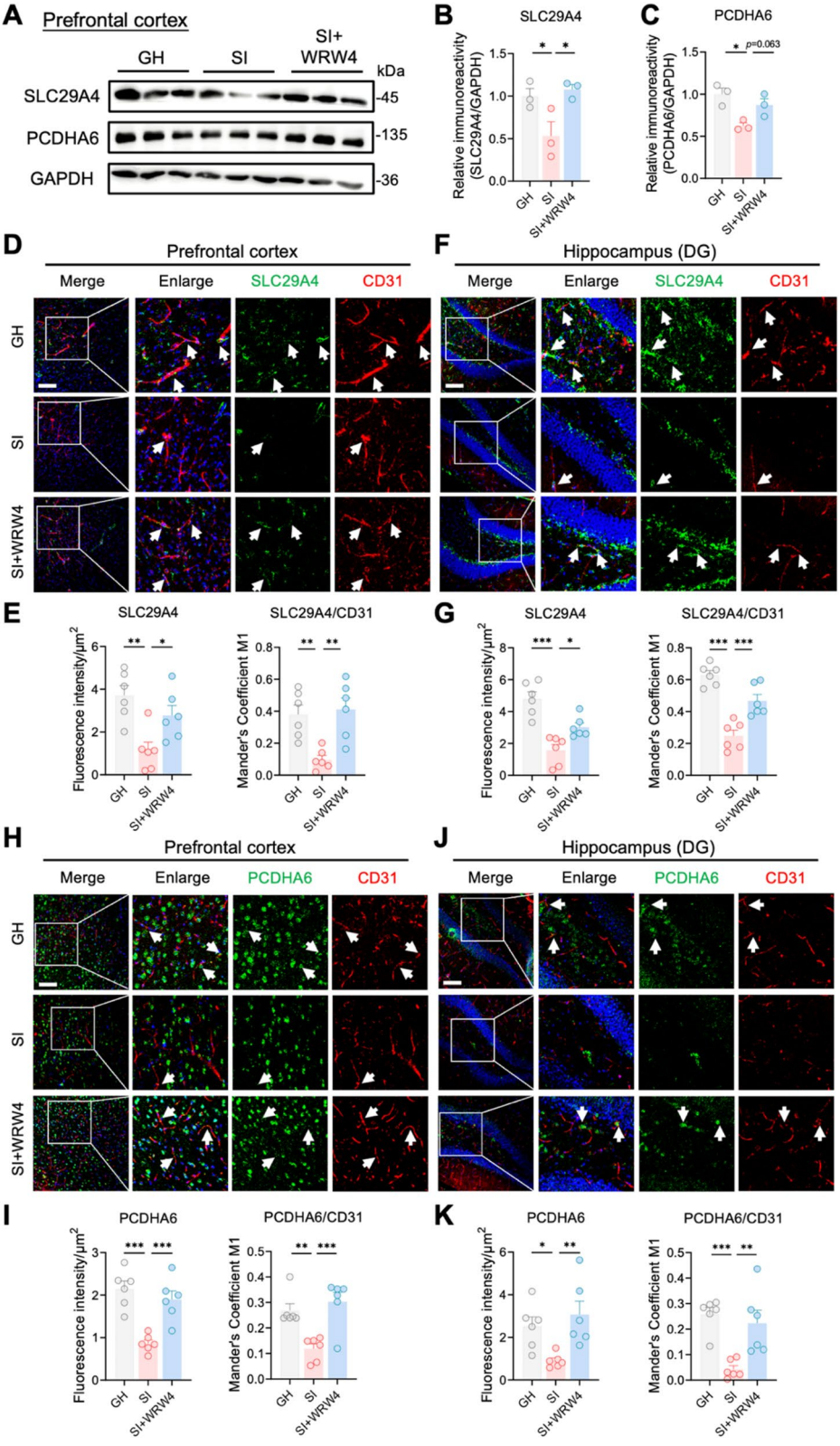

Fig. 7 (See legend on next page.)

(See figure on previous page.)

Fig. 7 WRW4 treatment upregulates the protein expression of SLC29A4 and PCDHA6 in the PFC and hippocampal DG region of SI mice. **A.** Representative images of Western blot analysis showing the expression levels of SLC29A4 and PCDHA6 in the PFC of GH, SI, and WRW4-treated SI mice. **B**, **C.** Quantification of the immunoreactivity of the blots, normalized against GAPDH. **D**, **F**, **H**, **J.** Immunofluorescence staining was performed to detect the expression of SLC29A4 and PCDHA6 in brain endothelial cells. Serial sections were stained for SLC29A4 or PCDHA6 using rabbit anti-SLC29A4 or anti-PCDHA6 antibodies, followed by Alexa Fluor 488-conjugated anti-rabbit IgG (green). Subsequently, the sections were stained with a rat anti-CD31 antibody, followed by Alexa Fluor 555-conjugated anti-rat IgG (red). Cell nuclei were counterstained with DAPI (blue). Scale bar, 100 μm. Selected areas of the PFC (**D**, **H**) and the hippocampal DG region (**F**, **J)** are magnified fivefold and presented as combined and individual fluorescence stains. The white arrow indicates the colocalization of SLC29A4 or PCDHA6 with CD31. Quantification of the fluorescence intensity of SLC29A4 or PCDHA6 and Manders' coefficient M1 (the fraction of SLC29A4 or PCDHA6 colocalized with CD31) in the PFC (**E**, **I**) and DG (**G**, **K**) are shown. Results are expressed as the mean ± SEM, based on two individual fields for each region, using three mice per group. * $p < 0.05$, ** $p < 0.01$, *** $p < 0.001$. GH, group-housed; SI, socially isolated; PFC, prefrontal cortex; DG, dentate gyrus

damaging the BBB [28]. These findings suggest that CAMs play a significant role in vascular function and BBB integrity under both physiological and pathological conditions, with their effects potentially shifting from protective to harmful depending on the disease's stage of progression. This study found that social isolation leads to an increase in the number of CAMs in the brains of mice, which was accompanied by elevated expression of FPR2. Given that FPR2 is a chemoattractant receptor that induces cell migration upon activation by specific ligands [37]. Furthermore, there is evidence of a chronic and sustained inflammatory response in the periphery and the brain of SI model mice [47, 81, 82]. Analysis of transcriptional data from brain tissue and peripheral blood of MDD patients revealed an upregulation of genes and pathways associated with inflammation. Based on the above evidence, we speculate that the increase of CAMs may be linked to FPR2 expression, which could promote their migration to blood vessels. This suggests that CAMs may play a detrimental role in BBB integrity in SI mice. In addition, analysis of RNA-seq results demonstrated that FPR2 inhibition leads to the enrichment and upregulation of the pathway related to the positive regulation of blood pressure in the brains of SI mice, implying that antagonizing FPR2 may contribute to the antidepressant effect by modulating vascular function. Whether this effect is mediated through the regulation of CAMs and the mechanism involved requires further investigation.

Disruption of the BBB integrity, resulting in increased permeability, is one of the crucial factors contributing to depressive-like behavior [22, 79, 80]. The BBB's integrity and permeability depend on the tight interactions between adjacent brain vascular endothelial cells, which are regulated by junctional complexes formed by various molecules, including tight junction and adhesion proteins. Menard et al. reported that chronic social stress compromises BBB integrity by reducing the tight junction protein Claudin-5, facilitating peripheral IL-6 translocation across the BBB, and contributing to depression [23]. They also found that targeted disruption of the BBB in the PFC of female mice induces depressive and anxiety-like behaviors [22]. These findings suggest a link between BBB damage and the onset of depression. However, the precise mechanisms underlying social isolation-induced depressive behaviors and BBB disruption remain unclear. Wu et al. reported a relationship between social isolation-induced anxiety-like behaviors and BBB integrity. They found that chronic childhood social isolation impairs BBB permeability and induces neuroinflammation in the amygdala by recruiting peripheral cytokines and activating microglia, which consequently triggers anxiety-like behaviors in female mice [83]. Our findings demonstrate that peripheral inhibition of FPR2 can mitigate BBB damage induced by social isolation by preserving BBB integrity. The integrity of the BBB is crucial for maintaining normal neuronal activity and function [25]. Our immunofluorescence staining results reveal significant albumin leakage in the brains of SI mice, which can cause edema around blood vessels, impair blood flow, and lead to neuronal damage and degeneration [84]. Therefore, the increase in FPR2 expression in CAMs within the brains of SI mice may indirectly contribute to the reduction of synaptic proteins and neuronal death by exacerbating BBB and vascular endothelial damage. Additionally, RNA sequencing revealed that the inhibition of FPR2 reversed the decline in transcript levels of endothelial cell-specific genes associated with tight junctions and material transport in the brains of SI model mice. It also restored the dysregulated expression of genes related to cognitive function and neurodevelopment in neurons. The FPR2 in CAMs may not directly induce changes in the transcription levels of endothelial cells and neurons; instead, it likely promotes the activation and migration of CAMs, leading to brain endothelial damage and compromising the integrity of the BBB, which, in turn, affects neuronal function. However, the exact mechanism by which FPR2 in CAMs regulates endothelial cell and neuronal function requires further experimental verification. Furthermore, the role of FPR2 expressed by brain parenchymal microglia in BBB damage caused by social isolation remains an unresolved question, warranting further exploration in future studies.

Furthermore, BBB transporters play a crucial role in mediating the transport of substances, such as macromolecules and hydrophilic compounds, between the periphery circulation and the brain. SLC29A4, the

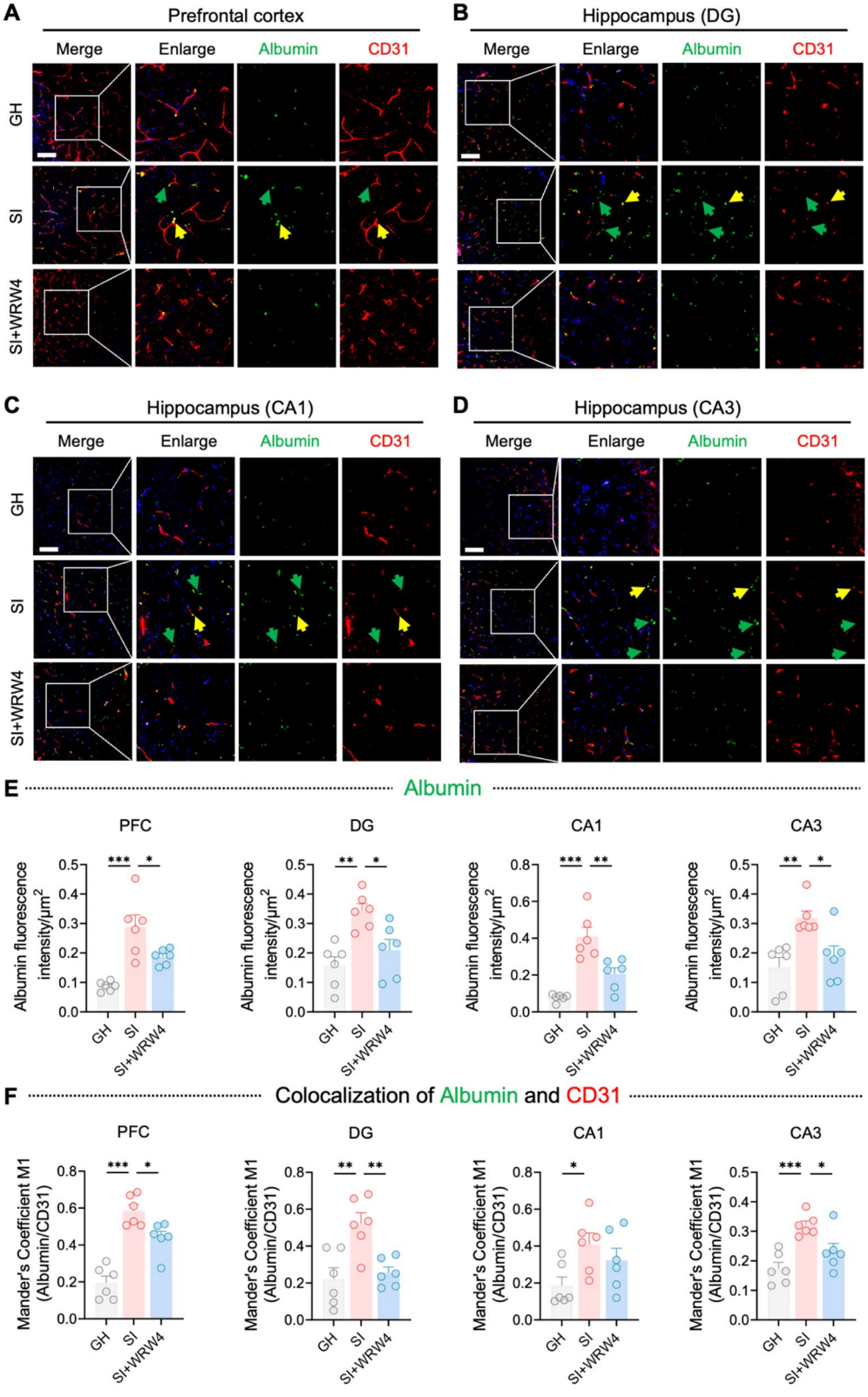

Fig. 8 (See legend on next page.)

(See figure on previous page.)

Fig. 8 WRW4 treatment alleviates the increased albumin leakage into the PFC and hippocampus of SI mice. **A-D.** Immunofluorescence staining was conducted to assess albumin leakage in the PFC and hippocampus of the brain. Serial sections from GH, SI, and WRW4-treated SI mice were stained for albumin using a rabbit anti-albumin antibody, followed by Alexa Fluor 488-conjugated anti-rabbit IgG (green). Subsequently, the sections were stained with a rat anti-CD31 antibody, followed by Alexa Fluor 555-conjugated anti-rat IgG (red). Cell nuclei were counterstained with DAPI (blue). Scale bar, 100 μm. Selected areas of the PFC (**A**) and the hippocampal regions, including the DG (**B**), CA1 (**C**), and CA3 (**D**), are magnified five times and presented as combined and individual fluorescence stains. The yellow arrow indicates the colocalization of albumin and CD31, while the green arrow marks the leakage of albumin into the brain parenchyma. **E.** Quantification of the fluorescence intensity of albumin in the PFC and hippocampus is presented. **F.** Quantification of Manders' coefficient M1 (the fraction of albumin colocalizing with CD31) in the PFC and hippocampus is also shown. Results are expressed as the mean ± SEM, based on two individual fields for each region, using three mice per group. * $p < 0.05$, ** $p < 0.01$, *** $p < 0.001$. GH, group-housed; SI, socially isolated; PFC, prefrontal cortex; DG, dentate gyrus; CA1, cornu ammonus-1; CA3, cornu ammonus-3

plasma membrane monoamine transporter (PMAT), is expressed in neurons and arachnoid endothelial cells within the brain. As the primary uptake$_2$ transporter, it can transport monoamine neurotransmitters, including serotonin, dopamine, and norepinephrine, with low affinity but high capacity. This mechanism enhances monoamine neurotransmitters' uptake, primarily mediated by uptake$_1$ transporters [85]. Studies have demonstrated that pharmacological intervention to inhibit SLC29A4 can strengthen the efficacy of SSRIs by reducing serotonin uptake and clearance, thereby improving antidepressant-like effects [86]. Notably, recent research has shown that the knockout of *Slc29a4* or *Sert* diminished the inhibitory effect of ketamine on serotonin clearance in mice, resulting in the loss of ketamine's antidepressant-like effects [87]. In addition, Adamsen et al. discovered that individuals with ASD exhibit a higher incidence of three rare non-synonymous mutations in the *Slc29a4* gene, two of which lead to functional impairment of SLC29A4 [88]. These findings suggest that SLC29A4 may play a role in the pathogenesis of mental disorders. Further research is needed to clarify its specific role and underlying mechanisms. Our study found that peripheral administration of WRW4 reverses the decrease in SLC29A4 expression in mouse brain microvascular endothelial cells caused by social isolation. While we speculate that this effect may be attributed to the protective influence of FPR2 inhibition on the BBB, we do not rule out the possibility that SLC29A4 may also be involved in the ameliorative effects of WRW4 on depressive and anxiety-like behaviors. No research has yet explored the impact of SLC29A4 in brain microvessels on monoamine transmitter transport between the periphery and the brain under either physiological or pathological conditions.

Our study demonstrated that social isolation induces alterations in the expression of several PCDHs in the mouse brain. PCDHs, which belong to the cadherin superfamily, are a class of cell adhesion molecules that play a crucial role in cell-cell communication [89]. Vadodaria et al. analyzed data from over 800 patients with MDD. They found that the transcriptional levels of the two essential protocadherin genes, PCDHA6 and PCDHA8, were significantly lower in serotonergic neurons of the SSRI non-remission group compared to those in healthy individuals and the SSRI-treated remission group. Deletion of *Pcdha6* or *Pcdha8* led to changes in the growth and morphology of serotonergic neurons, and these changes were linked to SSRI resistance in MDD patients [76]. Our investigation specifically aimed to verify the changes in PCDHA6 in the brains of SI mice. We confirmed that treatment with WRW4 can reverse the decrease in PCDHA6 expression observed in brain microvascular endothelial cells, particularly in neurons, resulting from social isolation. These findings suggest that protocadherins, particularly PCDHA6, may play a role in the pathogenesis of depression, including social isolation-induced depression, as well as in the efficacy of SSRI treatment.

FPR2 is a promising therapeutic target for various diseases. It has numerous ligands, and its binding with different ligands can elicit chemotaxis, migration, anti-inflammatory, or pro-inflammatory responses [37]. Research on the impact of pharmacological interventions or genetic knockout of FPR2 on depressive-like behaviors has yielded inconsistent results. ICV injection of the endogenous FPR2 agonist RvD1 exhibits antidepressant effects, while *Fpr2/3* knockout has also been shown to alleviate depressive-like behavior in mouse models of depression. Our study revealed that peripheral or central administration of the FPR2 antagonist WRW4 mitigates depressive and anxiety-like behaviors induced by social isolation in mice. Our previous studies found that *Fpr2* knockout can alleviate learning and cognitive deficits in Alzheimer's disease model mice [90]. These findings indicate whether the inhibiting or activation of FPR2 alleviates disease progression may be contingent upon the stage of the disease, the expression levels and balance of FPR2 and its endogenous ligands, as well as the specific cell types involved.

In conclusion, the present study demonstrates that FPR2 expression is upregulated in CAMs of socially isolated mice, as well as in ovFPC of MDD patients and PBMCs from individuals experiencing severe depressive episodes. Both peripheral and central administration of low doses of the FPR2 antagonist WRW4 attenuated depressive and anxiety-like behaviors induced by social isolation in mice. Moreover, peripheral WRW4 treatment reduced the increase of CAMs, mitigated the glial cell

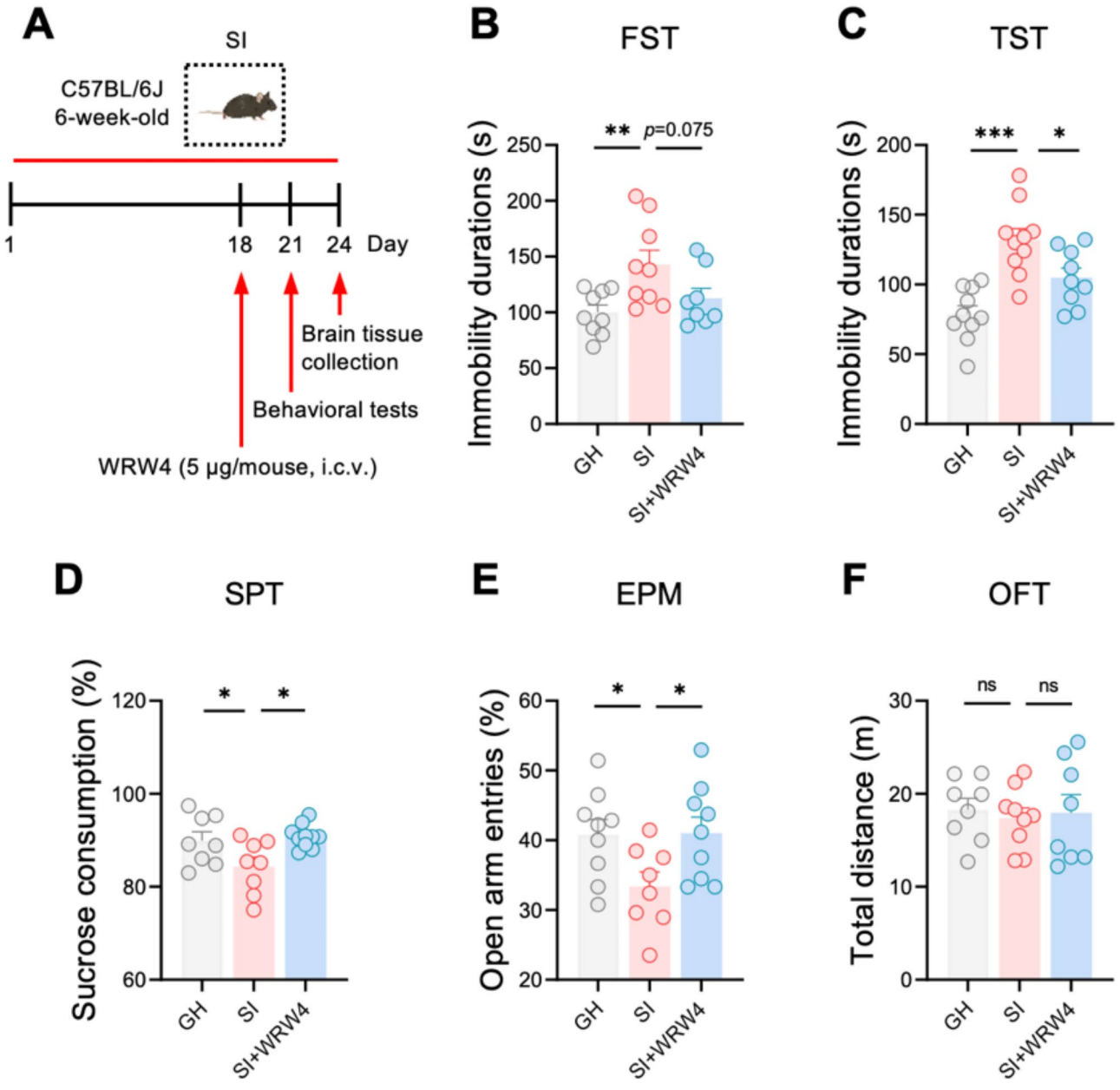

Fig. 9 ICV injection of WRW4 alleviates depressive and anxiety-like behaviors in SI mice. **A.** Schematic representation of the experimental procedure for the ICV injection of WRW4 to the social isolation model mice. **B**, **C.** WRW4 treatment significantly decreased the immobility time in the forced swim test (FST) and the tail suspension test (TST) in SI mice. **D.** WRW4 treatment increased the percentage of sucrose uptake in the sucrose preference test (SPT) in SI mice. **E.** WRW4 treatment increased the percentage of SI mice entering the open arms of the elevated plus maze (EPM) test. **F.** WRW4 treatment did not affect the total movement distance of SI mice in the open field test (OFT). Results are expressed as mean ± SEM, with 8–10 mice per group. * $p < 0.05$, ** $p < 0.01$, *** $p < 0.001$. GH, group-housed; SI, socially isolated; i.c.v, intracerebroventricular

activation, preserved neuronal function, and ameliorated BBB damage associated with social isolation in mice. Further investigation into the pathological mechanism of FPR2 in depression may uncover potential therapeutic targets, while precise modulation of FPR2 may yield novel strategies for the treatment of MDD.

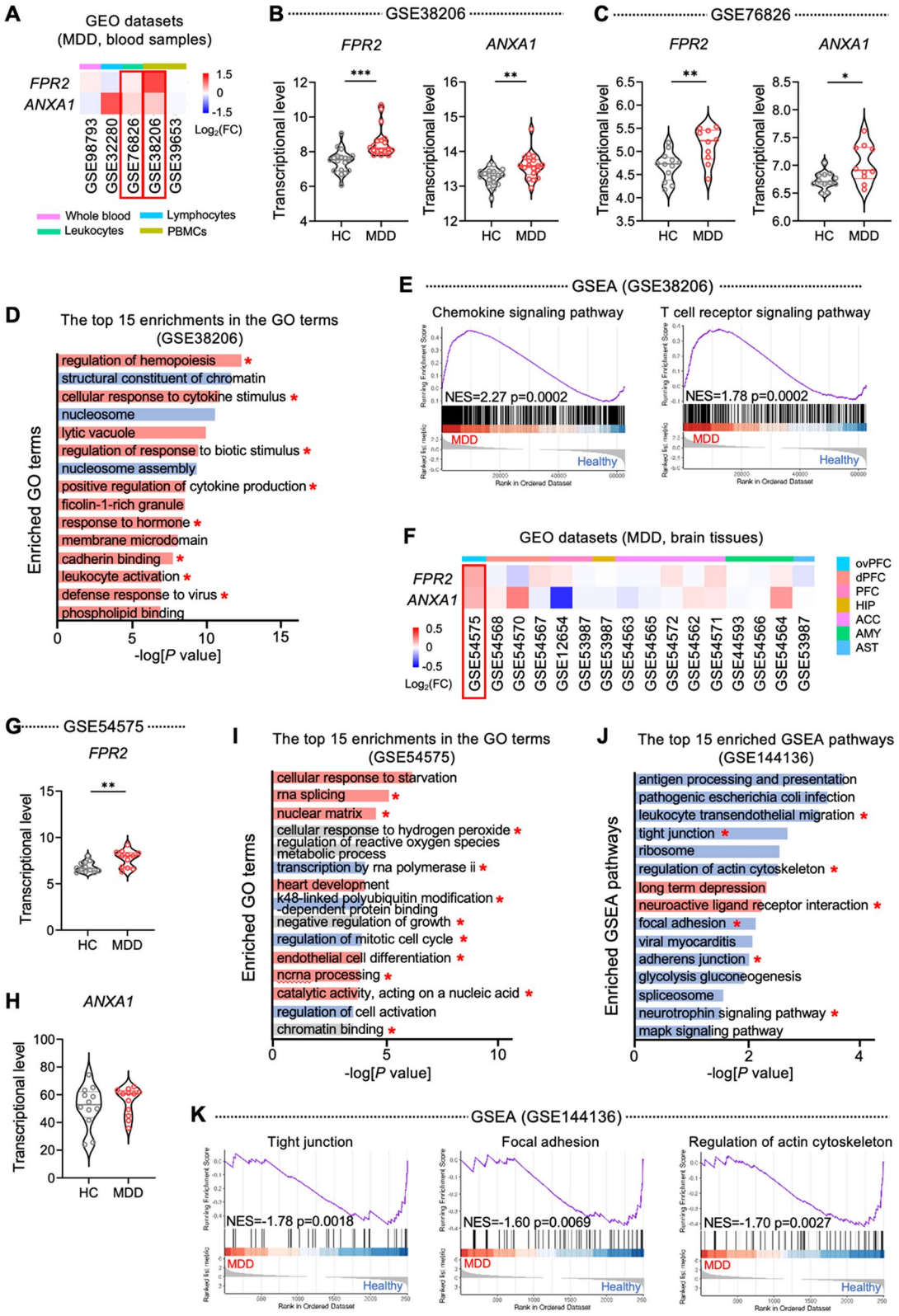

Fig. 10 (See legend on next page.)

(See figure on previous page.)

Fig. 10 Upregulation of *FPR2* and/or *ANXA1* transcriptional levels in the ovPFC and PBMCs of patients with MDD. **A.** Heat map showing the alterations in transcription levels of *FPR2* and *ANXA1* in peripheral whole blood, lymphocytes, leukocytes, and PBMCs of MDD patients compared to healthy controls (HCs), with transcriptome data derived from the NCBI GEO database. **B**, **C.** Assessment of the transcriptional levels of *FPR2* and *ANXA1* in PBMCs (accession number: GSE38206) and leukocytes (GSE76826) from MDD patients and HCs using quantile normalized values. **D.** Gene ontology (GO) analysis of differentially expressed genes (DEGs, absolute fold change [FC] > 1.50, $q < 0.05$, MDD vs. HCs) from GSE38206, displaying the top 15 differentially regulated pathways ranked by *p*-value, with asterisks indicating categories related to infection and immune responses. **E.** Gene set enrichment analysis (GSEA) results for GSE38206 showed upregulation of genes in the chemokine and T cell receptor signaling pathways in the PBMCs of MDD patients. **F.** Heat map illustrating the alterations in transcription levels of *FPR2* and *ANXA1* in various brain regions of MDD patients compared to HC's. **G**, **H.** Evaluation of transcriptional levels of *FPR2* and *ANXA1* in the ovPFC (GSE54575) of MDD patients and HCs using quantile normalized values. **I.** GO analysis of DEGs (absolute FC > 1.20, $p < 0.05$, MDD vs. HCs) from GSE54575, presenting the top 15 differentially regulated pathways ranked by *p*-value, with asterisks marking pathways related to protein synthesis or degradation and endothelial cell function. **J.** GSEA of transcriptome data of brain endothelial cell clusters in single-nucleus (sn)-RNA seq data (GSE144136) from the PFC of MDD patients and HCs. The top 15 differentially regulated pathways, ranked by *p*-value, are shown, with asterisks highlighting endothelial function-related pathways. **K.** GSEA results showed downregulation of genes in the tight junction, focal adhesion, and regulation of actin cytoskeleton in the PFC brain endothelial cells of MDD patients. Results are expressed as the mean ± SEM. * $p < 0.05$, ** $p < 0.01$, *** $p < 0.001$. ovPFC, orbital ventral prefrontal cortex; PBMCs, peripheral blood mononuclear cells; dPFC, dorsal prefrontal cortex; PFC, prefrontal cortex; HIP, hippocampus; ACC, anterior cingulate cortex; AMY, amygdala; AST, associative striatum

Abbreviations

ACC	Anterior cingulate cortex
AMY	Amygdala
ASD	Autism spectrum disorders
AST	Associative striatum
BBB	Blood-brain barrier
BP	Biological processes
CAMs	Capillary-associated microglia
CAMK2D	Calcium/calmodulin-dependent protein kinase II delta
CC	Cellular components
CNS	Central nervous system
DG	Dentate gyrus
DEGs	Differentially expressed genes
EPM	Elevated plus maze test
FC	Fold change
FPR2	Formyl peptide receptor 2
FST	Forced swim test
GEO	Gene expression omnibus
GFAP	Glial fibrillary acidic protein
GH	Group-housed
GO	Gene ontology
GSEA	Gene set enrichment analysis
HIP	Hippocampus
ICV	Intracerebroventricular
MF	Molecular functions
MDD	Major depressive disorder
NCBI	National Center for Biotechnology Information
NVU	Neurovascular unit
ovPFC	Orbital ventral PFC
OFT	Open field test
PBS	Phosphate-buffered saline
PBMCs	Peripheral blood mononuclear cells
PCDHs	Protocadherins
PFA	Paraformaldehyde
PFC	Prefrontal cortex
PSD95	Post-synaptic density 95
SI	Social isolation/socially isolated
SPT	Sucrose preference test
SSRI	Selective serotonin reuptake inhibitor
SYN	Synaptophysin
TST	Tail suspension test
WT	Wild-type

Supplementary Information

The online version contains supplementary material available at https://doi.org/10.1186/s12974-025-03408-4.

Supplementary Material 1

Supplementary Material 2

Supplementary Material 3

Supplementary Material 4

Acknowledgements
The graphical abstract and behavioral testing cartoons depicted in Fig. 1 were created using Figdraw.

Author contributions
JYZ, HQW, WNW, LLW, MZQ, LFZ, ZL, and YJC performed the experiments. JYZ, HQW, WNW, and LLW processed and analyzed the data. JYZ and YY wrote the manuscript. JYZ and YY conceived and designed the study. All authors have read and approved the final manuscript.

Funding
This research was funded by grants from the Natural Science Foundation of Shanghai (Grant 22ZR1434700), the National Natural Science Foundation of China (Grant 81870835), and the Hui-Chun Chin and Tsung-Dao Lee Chinese Undergraduate Research Endowment.

Data availability
No datasets were generated or analysed during the current study.

Declarations

Ethics approval and consent to participate
All animal experiments were performed according to the guidelines of the National Institutes of Health Guide for the Care and Use of Laboratory Animals, with procedures approved by the Biological Research Ethics Committee of Shanghai Jiao Tong University.

Consent for publication
Not applicable.

Competing interests
The authors declare no competing interests.

Author details
[1]Shanghai Frontiers Science Center of Drug Target Identification and Delivery, Engineering Research Center of Cell and Therapeutic Antibody, Ministry of Education, School of Pharmaceutical Sciences, Shanghai Jiao Tong University, Shanghai 200240, China
[2]School of Pharmaceutical Science, Southern Medical University, Guangzhou 510515, China
[3]Chemical Biology Research Center, School of Pharmaceutical Sciences, Wenzhou Medical University, Wenzhou 325035, China

Received: 21 October 2024 / Accepted: 4 March 2025
Published online: 13 March 2025

References

1. Cacioppo JT, Hawkley LC. Perceived social isolation and cognition. Trends Cogn Sci. 2009;13:447–54.
2. Valtorta NK, Kanaan M, Gilbody S, Ronzi S, Hanratty B. Loneliness and social isolation as risk factors for coronary heart disease and stroke: systematic review and meta-analysis of longitudinal observational studies. Heart. 2016;102:1009–16.
3. Friedler B, Crapser J, McCullough L. One is the deadliest number: the detrimental effects of social isolation on cerebrovascular diseases and cognition. Acta Neuropathol. 2015;129:493–509.
4. Steptoe A, Shankar A, Demakakos P, Wardle J. Social isolation, loneliness, and all-cause mortality in older men and women. Proc Natl Acad Sci U S A. 2013;110:5797–801.
5. Kawachi I, Berkman LF. Social ties and mental health. J Urban Health. 2001;78:458–67.
6. Achterbergh L, Pitman A, Birken M, Pearce E, Sno H, Johnson S. The experience of loneliness among young people with depression: a qualitative meta-synthesis of the literature. BMC Psychiatry 2020, 20.
7. van den Brink RHS, Schutter N, Hanssen DJC, Elzinga BM, Rabeling-Keus IM, Stek ML, Comijs HC, Penninx B, Oude Voshaar RC. Prognostic significance of social network, social support and loneliness for course of major depressive disorder in adulthood and old age. Epidemiol Psychiatr Sci. 2018;27:266–77.
8. Marx W, Penninx B, Solmi M, Furukawa TA, Firth J, Carvalho AF, Berk M. Major depressive disorder. Nat Rev Dis Primers. 2023;9:44.
9. Fancourt D, Steptoe A, Bu FF. Trajectories of anxiety and depressive symptoms during enforced isolation due to COVID-19 in England: a longitudinal observational study. Lancet Psychiatry. 2021;8:141–9.
10. Simard J, Volicer L. Loneliness and isolation in Long-term care and the COVID-19 pandemic. J Am Med Dir Assoc. 2020;21:966–7.
11. Huang Y, Wang Y, Wang H, Liu Z, Yu X, Yan J, Yu Y, Kou C, Xu X, Lu J, et al. Prevalence of mental disorders in China: a cross-sectional epidemiological study. Lancet Psychiatry. 2019;6:211–24.
12. Warden D, Rush AJ, Trivedi MH, Fava M, Wisniewski SR. The STAR*D project results: a comprehensive review of findings. Curr Psychiatry Rep. 2007;9:449–59.
13. Uher R, Tansey KE, Dew T, Maier W, Mors O, Hauser J, Dernovsek MZ, Henigsberg N, Souery D, Farmer A, McGuffin P. An inflammatory biomarker as a differential predictor of outcome of depression treatment with Escitalopram and Nortriptyline. Am J Psychiatry. 2014;171:1278–86.
14. Arteaga-Henriquez G, Simon MS, Burger B, Weidinger E, Wijkhuijs A, Arolt V, Birkenhager TK, Musil R, Muller N, Drexhage HA. Low-Grade inflammation as a predictor of antidepressant and Anti-Inflammatory therapy response in MDD patients: A systematic review of the literature in combination with an analysis of experimental data collected in the EU-MOODINFLAME consortium. Front Psychiatry. 2019;10:458.
15. Drevets WC, Wittenberg GM, Bullmore ET, Manji HK. Immune targets for therapeutic development in depression: towards precision medicine. Nat Rev Drug Discov. 2022;21:224–44.
16. Miller AH, Raison CL. The role of inflammation in depression: from evolutionary imperative to modern treatment target. Nat Rev Immunol. 2016;16:22–34.
17. Chan KL, Poller WC, Swirski FK, Russo SJ. Central regulation of stress-evoked peripheral immune responses. Nat Rev Neurosci. 2023;24:591–604.
18. Branchi I, Poggini S, Capuron L, Benedetti F, Poletti S, Tamouza R, Drexhage HA, Penninx B, Pariante CM, European College of Neuropsychopharmacology ImmunoNeuroPsychiatry Thematic Working, Marion G. L: Brain-immune crosstalk in the treatment of major depressive disorder. Eur Neuropsychopharmacol 2021, 45:89–107.
19. Enache D, Pariante CM, Mondelli V. Markers of central inflammation in major depressive disorder: A systematic review and meta-analysis of studies examining cerebrospinal fluid, positron emission tomography and post-mortem brain tissue. Brain Behav Immun. 2019;81:24–40.
20. Miller AH, Maletic V, Raison CL. Inflammation and its discontents: the role of cytokines in the pathophysiology of major depression. Biol Psychiatry. 2009;65:732–41.
21. Dudek KA, Dion-Albert L, Lebel M, LeClair K, Labrecque S, Tuck E, Ferrer Perez C, Golden SA, Tamminga C, Turecki G, et al. Molecular adaptations of the blood-brain barrier promote stress resilience vs. depression. Proc Natl Acad Sci U S A. 2020;117:3326–36.
22. Dion-Albert L, Cadoret A, Doney E, Kaufmann FN, Dudek KA, Daigle B, Parise LF, Cathomas F, Samba N, Hudson N, et al. Vascular and blood-brain barrier-related changes underlie stress responses and resilience in female mice and depression in human tissue. Nat Commun. 2022;13:164.
23. Menard C, Pfau ML, Hodes GE, Kana V, Wang VX, Bouchard S, Takahashi A, Flanigan ME, Aleyasin H, LeClair KB, et al. Social stress induces neurovascular pathology promoting depression. Nat Neurosci. 2017;20:1752–60.
24. Abbott NJ, Patabendige AA, Dolman DE, Yusof SR, Begley DJ. Structure and function of the blood-brain barrier. Neurobiol Dis. 2010;37:13–25.
25. Wu D, Chen Q, Chen X, Han F, Chen Z, Wang Y. The blood-brain barrier: structure, regulation, and drug delivery. Signal Transduct Target Ther. 2023;8:217.
26. Obermeier B, Daneman R, Ransohoff RM. Development, maintenance and disruption of the blood-brain barrier. Nat Med. 2013;19:1584–96.
27. Mondo E, Becker SC, Kautzman AG, Schifferer M, Baer CE, Chen J, Huang EJ, Simons M, Schafer DP. A developmental analysis of juxtavascular microglia dynamics and interactions with the vasculature. J Neurosci. 2020;40:6503–21.
28. Haruwaka K, Ikegami A, Tachibana Y, Ohno N, Konishi H, Hashimoto A, Matsumoto M, Kato D, Ono R, Kiyama H, et al. Dual microglia effects on blood brain barrier permeability induced by systemic inflammation. Nat Commun. 2019;10:5816.
29. Bisht K, Okojie KA, Sharma K, Lentferink DH, Sun YY, Chen HR, Uweru JO, Amancherla S, Calcuttawala Z, Campos-Salazar AB, et al. Capillary-associated microglia regulate vascular structure and function through PANX1-P2RY12 coupling in mice. Nat Commun. 2021;12:5289.
30. Ye RD, Boulay F, Wang JM, Dahlgren C, Gerard C, Parmentier M, Serhan CN, Murphy PM. International union of basic and clinical pharmacology. LXXIII. Nomenclature for the formyl peptide receptor (FPR) family. Pharmacol Rev. 2009;61:119–61.
31. Becker EL, Forouhar FA, Grunnet ML, Boulay F, Tardif M, Bormann BJ, Sodja D, Ye RD, Woska JR Jr., Murphy PM. Broad immunocytochemical localization of the formylpeptide receptor in human organs, tissues, and cells. Cell Tissue Res. 1998;292:129–35.
32. Liu GJ, Tao T, Wang H, Zhou Y, Gao X, Gao YY, Hang CH, Li W. Functions of resolvin D1-ALX/FPR2 receptor interaction in the hemoglobin-induced microglial inflammatory response and neuronal injury. J Neuroinflammation. 2020;17:239.
33. Smole U, Gour N, Phelan J, Hofer G, Kohler C, Kratzer B, Tauber PA, Xiao X, Yao N, Dvorak J, et al. Serum amyloid A is a soluble pattern recognition receptor that drives type 2 immunity. Nat Immunol. 2020;21:756–65.
34. Qin CX, Norling LV, Vecchio EA, Brennan EP, May LT, Wootten D, Godson C, Perretti M, Ritchie RH. Formylpeptide receptor 2: nomenclature, structure, signalling and translational perspectives: IUPHAR review 35. Br J Pharmacol. 2022;179:4617–39.
35. Gobbetti T, Coldewey SM, Chen J, McArthur S, le Faouder P, Cenac N, Flower RJ, Thiemermann C, Perretti M. Nonredundant protective properties of FPR2/ALX in polymicrobial murine sepsis. Proc Natl Acad Sci U S A. 2014;111:18685–90.
36. Trojan E, Bryniarska N, Leskiewicz M, Regulska M, Chamera K, Szuster-Gluszczak M, Leopoldo M, Lacivita E, Basta-Kaim A. The contribution of formyl peptide receptor dysfunction to the course of neuroinflammation: A potential role in the brain pathology. Curr Neuropharmacol. 2020;18:229–49.
37. He HQ, Ye RD. The formyl peptide receptors: diversity of ligands and mechanism for recognition. Molecules 2017, 22.
38. Zhu Y, Lin X, Zong X, Han S, Wang M, Su Y, Ma L, Chu X, Yi C, Zhao Q, Wu B. Structural basis of FPR2 in recognition of Abeta(42) and neuroprotection by humanin. Nat Commun. 2022;13:1775.
39. Zhuang Y, Wang L, Guo J, Sun D, Wang Y, Liu W, Xu HE, Zhang C. Molecular recognition of formylpeptides and diverse agonists by the formylpeptide receptors FPR1 and FPR2. Nat Commun. 2022;13:1054.
40. Wu MY, Ge YJ, Wang EJ, Liao QW, Ren ZY, Yu Y, Zhu G, Liu CP, Zhang MN, Su H, et al. Enhancement of efferocytosis through biased FPR2 signaling attenuates intestinal inflammation. EMBO Mol Med. 2023;15:e17815.
41. Zhang S, Gong H, Ge Y, Ye RD. Biased allosteric modulation of formyl peptide receptor 2 leads to distinct receptor conformational States for pro- and anti-inflammatory signaling. Pharmacol Res. 2020;161:105117.
42. Cooray SN, Gobbetti T, Montero-Melendez T, McArthur S, Thompson D, Clark AJ, Flower RJ, Perretti M. Ligand-specific conformational change of the G-protein-coupled receptor ALX/FPR2 determines proresolving functional responses. Proc Natl Acad Sci U S A. 2013;110:18232–7.
43. Deyama S, Ishikawa Y, Yoshikawa K, Shimoda K, Ide S, Satoh M, Minami M. Resolvin D1 and D2 reverse Lipopolysaccharide-Induced Depression-Like behaviors through the mTORC1 signaling pathway. Int J Neuropsychopharmacol. 2017;20:575–84.
44. Ishikawa Y, Deyama S, Shimoda K, Yoshikawa K, Ide S, Satoh M, Minami M. Rapid and sustained antidepressant effects of resolvin D1 and D2 in a chronic unpredictable stress model. Behav Brain Res. 2017;332:233–6.

45. Gallo I, Rattazzi L, Piras G, Gobbetti T, Panza E, Perretti M, Dalley JW, D'Acquisto F. Formyl peptide receptor as a novel therapeutic target for anxiety-related disorders. PLoS ONE. 2014;9:e114626.
46. Peritore AF, Crupi R, Scuto M, Gugliandolo E, Siracusa R, Impellizzeri D, Cordaro M, D'Amico R, Fusco R, Di Paola R, Cuzzocrea S. The role of Annexin A1 and formyl peptide receptor 2/3 signaling in chronic Corticosterone-Induced Depression-Like behaviors and impairment in Hippocampal-Dependent memory. CNS Neurol Disord Drug Targets. 2020;19:27–43.
47. Lee JS, Lee SB, Kim DW, Shin N, Jeong SJ, Yang CH, Son CG. Social isolation-related depression accelerates ethanol intake via microglia-derived neuroinflammation. Sci Adv. 2021;7:eabj3400.
48. Xu X, Gao W, Li L, Hao J, Yang B, Wang T, Li L, Bai X, Li F, Ren H, et al. Annexin A1 protects against cerebral ischemia-reperfusion injury by modulating microglia/macrophage polarization via FPR2/ALX-dependent AMPK-mTOR pathway. J Neuroinflammation. 2021;18:119.
49. Girol AP, Mimura KK, Drewes CC, Bolonheis SM, Solito E, Farsky SH, Gil CD, Oliani SM. Anti-inflammatory mechanisms of the Annexin A1 protein and its mimetic peptide Ac2-26 in models of ocular inflammation in vivo and in vitro. J Immunol. 2013;190:5689–701.
50. Schroder N, Schaffrath A, Welter JA, Putzka T, Griep A, Ziegler P, Brandt E, Samer S, Heneka MT, Kaddatz H, et al. Inhibition of formyl peptide receptors improves the outcome in a mouse model of alzheimer disease. J Neuroinflammation. 2020;17:131.
51. Zhang H, Lin A, Gong P, Chen Y, Ye RD, Qian F, Zhang Y, Yu Y. The Chemokine-like receptor 1 deficiency improves cognitive deficits of AD mice and attenuates Tau hyperphosphorylation via regulating Tau seeding. J Neurosci. 2020;40:6991–7007.
52. Manders EMM, Verbeek FJ, Aten JA. Measurement of co-localization of objects in dual-colour confocal images. J Microsc. 1993;169:375–82.
53. Zinchuk V, Zinchuk O, Okada T. Quantitative colocalization analysis of multicolor confocal Immunofluorescence microscopy images: pushing pixels to explore biological phenomena. Acta Histochem Cytochem. 2007;40:101–11.
54. Clough E, Barrett T, Wilhite SE, Ledoux P, Evangelista C, Kim IF, Tomashevsky M, Marshall KA, Phillippy KH, Sherman PM, et al. NCBI GEO: archive for gene expression and epigenomics data sets: 23-year update. Nucleic Acids Res. 2024;52:D138–44.
55. Watanabe S, Al Omran A, Shao AS, Liang J. Social isolation model: A noninvasive rodent model of stress and anxiety. Jove-Journal of Visualized Experiments; 2022.
56. Kisler K, Nikolakopoulou AM, Zlokovic BV. Microglia have a grip on brain microvasculature. Nat Commun. 2021;12:5290.
57. Cui YH, Le Y, Zhang X, Gong W, Abe K, Sun R, Van Damme J, Proost P, Wang JM. Up-regulation of FPR2, a chemotactic receptor for amyloid beta 1–42 (A beta 42), in murine microglial cells by TNF alpha. Neurobiol Dis. 2002;10:366–77.
58. Liddelow SA, Guttenplan KA, Clarke LE, Bennett FC, Bohlen CJ, Schirmer L, Bennett ML, Munch AE, Chung WS, Peterson TC, et al. Neurotoxic reactive astrocytes are induced by activated microglia. Nature. 2017;541:481–7.
59. Cheng YT, Woo J, Luna-Figueroa E, Maleki E, Harmanci AS, Deneen B. Social deprivation induces astrocytic TRPA1-GABA suppression of hippocampal circuits. Neuron. 2023;111:1301–e13151305.
60. Ooigawa H, Nawashiro H, Fukui S, Otani N, Osumi A, Toyooka T, Shima K. The fate of Nissl-stained dark neurons following traumatic brain injury in rats: difference between neocortex and hippocampus regarding survival rate. Acta Neuropathol. 2006;112:471–81.
61. Munji RN, Soung AL, Weiner GA, Sohet F, Semple BD, Trivedi A, Gimlin K, Kotoda M, Korai M, Aydin S, et al. Profiling the mouse brain endothelial transcriptome in health and disease models reveals a core blood-brain barrier dysfunction module. Nat Neurosci. 2019;22:1892–902.
62. Engel K, Zhou M, Wang J. Identification and characterization of a novel monoamine transporter in the human brain. J Biol Chem. 2004;279:50042–9.
63. Nagy C, Maitra M, Tanti A, Suderman M, Theroux JF, Davoli MA, Perlman K, Yerko V, Wang YC, Tripathy SJ, et al. Single-nucleus transcriptomics of the prefrontal cortex in major depressive disorder implicates oligodendrocyte precursor cells and excitatory neurons. Nat Neurosci. 2020;23:771–81.
64. Chuang CF, King CE, Ho BW, Chien KY, Chang YC. Unbiased proteomic study of the axons of cultured rat cortical neurons. J Proteome Res. 2018;17:1953–66.
65. Nagao M, Ogata T, Sawada Y, Gotoh Y. Zbtb20 promotes astrocytogenesis during neocortical development. Nat Commun 2016, 7.
66. Dilling C, Roewer N, Förster CY, Burek M. Multiple protocadherins are expressed in brain microvascular endothelial cells and might play a role in tight junction protein regulation. J Cereb Blood Flow Metab. 2017;37:3391–400.
67. Geuens T, Bouhy D, Timmerman V. The HnRNP family: insights into their role in health and disease. Hum Genet. 2016;135:851–67.
68. Blalock EM, Geddes JW, Chen KC, Porter NM, Markesbery WR, Landfield PW. Incipient Alzheimer's disease: microarray correlation analyses reveal major transcriptional and tumor suppressor responses. Proc Natl Acad Sci U S A. 2004;101:2173–8.
69. Rigter PMF, de Konink C, Dunn MJ, Proietti Onori M, Humberson JB, Thomas M, Barnes C, Prada CE, Weaver KN, Ryan TD, et al. Role of CAMK2D in neurodevelopment and associated conditions. Am J Hum Genet. 2024;111:364–82.
70. Jones KA, Luo Y, Dukes-Rimsky L, Srivastava DP, Koul-Tewari R, Russell TA, Shapiro LP, Srivastava AK, Penzes P. Neurodevelopmental disorder-associated gene variants affect dendritic and synaptic structure. PLoS ONE 2018, 13.
71. Banerjee-Basu S, Packer A. SFARI gene: an evolving database for the autism research community. Dis Models Mech. 2010;3:133–5.
72. Thu CA, Chen WV, Rubinstein R, Chevee M, Wolcott HN, Felsovalyi KO, Tapia JC, Shapiro L, Honig B, Maniatis T. Single-cell identity generated by combinatorial homophilic interactions between alpha, beta, and gamma protocadherins. Cell. 2014;158:1045–59.
73. Mountoufaris G, Chen WV, Hirabayashi Y, O'Keeffe S, Chevee M, Nwakeze CL, Polleux F, Maniatis T. Multicluster Pcdh diversity is required for mouse olfactory neural circuit assembly. Science. 2017;356:411–4.
74. Lv X, Li S, Li J, Yu XY, Ge X, Li B, Hu S, Lin Y, Zhang S, Yang J, et al. Patterned cPCDH expression regulates the fine organization of the neocortex. Nature. 2022;612:503–11.
75. Ivanchenko MV, Hathaway DM, Klein AJ, Pan B, Strelkova O, De-la-Torre P, Wu X, Peters CW, Mulhall EM, Booth KT, et al. Mini-PCDH15 gene therapy rescues hearing in a mouse model of Usher syndrome type 1F. Nat Commun. 2023;14:2400.
76. Vadodaria KC, Ji Y, Skime M, Paquola AC, Nelson T, Hall-Flavin D, Heard KJ, Fredlender C, Deng Y, Elkins J, et al. Altered serotonergic circuitry in SSRI-resistant major depressive disorder patient-derived neurons. Mol Psychiatry. 2019;24:808–18.
77. Lago N, Kaufmann FN, Negro-Demontel ML, Ali-Ruiz D, Ghisleni G, Rego N, Arcas-Garcia A, Vitureira N, Jansen K, Souza LM, et al. CD300f immunoreceptor is associated with major depressive disorder and decreased microglial metabolic fitness. Proc Natl Acad Sci U S A. 2020;117:6651–62.
78. Kadriu B, Gold PW, Luckenbaugh DA, Lener MS, Ballard ED, Niciu MJ, Henter ID, Park LT, De Sousa RT, Yuan P, et al. Acute ketamine administration corrects abnormal inflammatory bone markers in major depressive disorder. Mol Psychiatry. 2018;23:1626–31.
79. Schiavone S, Mhillaj E, Neri M, Morgese MG, Tucci P, Bove M, Valentino M, Di Giovanni G, Pomara C, Turillazzi E, et al. Early loss of Blood-Brain barrier integrity precedes NOX2 elevation in the prefrontal cortex of an animal model of psychosis. Mol Neurobiol. 2017;54:2031–44.
80. Welcome MO, Mastorakis NE. Stress-induced blood brain barrier disruption: molecular mechanisms and signaling pathways. Pharmacol Res. 2020;157:104769.
81. Al Omran AJ, Shao AS, Watanabe S, Zhang ZY, Zhang JF, Xue C, Watanabe J, Davies DL, Shao XSM, Liang J. Social isolation induces neuroinflammation and microglia overactivation, while Dihydromyricetin prevents and improves them. J Neuroinflamm 2022, 19.
82. Hamilton A, Rizzo R, Brod S, Ono M, Perretti M, Cooper D, D'Acquisto F. The Immunomodulatory effects of social isolation in mice are linked to temperature control. Brain Behav Immun. 2022;102:179–94.
83. Wu X, Ding Z, Fan T, Wang K, Li S, Zhao J, Zhu W. Childhood social isolation causes anxiety-like behaviors via the damage of blood-brain barrier in amygdala in female mice. Front Cell Dev Biol. 2022;10:943067.
84. Sweeney MD, Sagare AP, Zlokovic BV. Blood-brain barrier breakdown in alzheimer disease and other neurodegenerative disorders. Nat Rev Neurol. 2018;14:133–50.
85. Vieira LS, Wang J. Brain plasma membrane monoamine transporter in health and disease. Handb Exp Pharmacol. 2021;266:253–80.
86. Horton RE, Apple DM, Owens WA, Baganz NL, Cano S, Mitchell NC, Vitela M, Gould GG, Koek W, Daws LC. Decynium-22 enhances SSRI-induced antidepressant-like effects in mice: Uncovering novel targets to treat depression. J Neurosci. 2013;33:10534–43.
87. Bowman MA, Vitela M, Clarke KM, Koek W, Daws LC. Serotonin transporter and plasma membrane monoamine transporter are necessary for the Antidepressant-Like effects of ketamine in mice. Int J Mol Sci 2020, 21.

88. Adamsen D, Ramaekers V, Ho HT, Britschgi C, Rufenacht V, Meili D, Bobrowski E, Philippe P, Nava C, Van Maldergem L, et al. Autism spectrum disorder associated with low serotonin in CSF and mutations in the SLC29A4 plasma membrane monoamine transporter (PMAT) gene. Mol Autism. 2014;5:43.
89. Jia Z, Wu Q. Clustered protocadherins emerge as novel susceptibility loci for mental disorders. Front Neurosci. 2020;14:587819.
90. Zhang H, Wang D, Gong P, Lin A, Zhang Y, Ye RD, Yu Y. Formyl peptide receptor 2 deficiency improves cognition and attenuates Tau hyperphosphorylation and astrogliosis in a mouse model of Alzheimer's disease. J Alzheimers Dis. 2019;67:169–79.

Publisher's note